DEVELOPMENT OF AN INTERFACIAL TRACER TEST FOR DNAPL ENTRAPPED IN DISCRETE FRACTURED ROCK

DEVELOPMENT OF AN INTERFACIAL TRACER TEST FOR DNAPL ENTRAPPED IN DISCRETE FRACTURED ROCK

by
BETHANY SEKERAK, Honours B.Sc.

A thesis
Submitted to the School of Graduate Studies
in Partial Fulfilment of the Requirements
for the Degree
Masters of Applied Science Degree

McMaster University

MASTERS OF APPLIED SCIENCE (2004) McMaster University
(Civil Engineering) Hamilton, Ontario

TITLE: Development of an Interfacial Tracer Test for DNAPL Entrapped in Discrete Fractured Rock.

AUTHOR: Bethany Sekerak, Honours B.Sc. (McMaster University)

SUPERVISOR: Professor S. Dickson

NUMBER OF PAGES: vii, 100

ABSTRACT

Denser-than-water, non-aqueous phase liquids (DNAPLs) are contaminants that pose a serious threat to groundwater quality because of their high toxicity and ease of mobility once released into the groundwater system. In order to effectively assess the risk to human and ecological health, and to select an appropriate remediation strategy, the DNAPL source zone must be accurately characterized. The area of the DNAPL-water interface is one feature commonly used to characterize the DNAPL source zone; it is significant as it measures the surface area available for DNAPL mass transfer into the groundwater causing contamination. Additionally, many remediation strategies depend on the inter-phase mass transfer. At present, interfacial tracer tests have been successful for determining the DNAPL-water interfacial area in unconsolidated porous media, yet no study has applied this technique to fractured rock systems. The purpose of this study was to develop an interfacial tracer technique for determining the DNAPL-water interfacial area, a_{nw}, in fractured rock environments. The experimental design involved four phases (1) characterizing two fracture planes using hydraulic and tracer studies, (2) trapping a known mass of a DNAPL, hydrofluoroether 7100 (HFE7100) in the fractured rock systems, (3) performing interfacial tracer tests with sodium dodecyl benzene sulphate, sodium dodecylbenzene sulphonate (SDBS) as the reactive tracer and acid yellow 17 as the non-reactive tracer to derive an a_{nw} measurement, and (4) verifying the a_{nw} value through visualization using digital image analysis. While the interfacial tracer technique was only applied to two unique fractures in this study, it demonstrates the

ability to obtain a measure of the DNAPL-water contact area, and offers an additional tool for the characterization of DNAPL source zones at the lab-scale; further work is required to evaluate the tracer test methodology for field applications.

ACKNOWLEGEMENTS

Funding for this research was provided by Natural Science and Engineering Research Council of Canada (NSERC), Canadian Foundation for Innovation, and Ontario Innovation Trust (OIT).

I would like to sincerely thank a number of people who have supported me throughout my masters program. Most importantly, I would like to extend my gratitude to my supervisor, Sarah Dickson who was an inspiration with her innovative ideas and enthusiasm. She provided sound guidance and endless support; even when the times were tough, her pep-talks always sent me back to the lab. I would also like to thank Dr. Jim Smith from the School of Geography and Geology for his advice and for lending me the use of his lab and tenisometer equipment.

I am grateful for the assistance of Peter Koudys and Anna Roberston, whose technical skills were invaluable in my laboratory experiments. Many undergraduate students, including Dave, Jenn, and Tammera were also a great help in the lab.

Many thanks to my fellow graduate students who were always ready discuss problems and offer solutions. In particular, I would like to thank Martina, who was a great help to me both in the lab and as moral support, and many other good friends, including Margaret, Tara, and Liz. You have made grad school especially memorable and I cherish our friendships. Finally, I would like to thank Mike for his abiding support and for being my energizer near the end when time was tight.

TABLE OF CONTENTS

Page

CHAPTER 1: INTRODUCTION 1
1.1. Research Goals and Objectives 4

CHAPTER 2: BACKGROUND 6
2.1. The Forces Governing DNAPL Movement 7
2.1.1. Capillary Force 7
2.1.2. Viscous Force 9
2.1.3. Gravitational Force 9
2.2. DNAPL Migration in Fractures 10
2.3. DNAPL Entrapment 11
2.3.1. Stability Measures for Entrapped DNAPL Mass 12
2.4. Interfacial Tracer Technique 12
2.4.1. Interfacial Tracer Technique -An Overview 13
2.4.2. Surfactant Adsorption at the DNAPL-Water Interface 14
2.4.3. Retardation Model & Interfacial Area Calculation 18
2.4.4. Reliability of the Retardation Model 20

CHAPTER 3: EXPERIMENTAL DESIGN 22
3.1. Fracture Plane Preparation 22
3.1.1. Rock Sample Preparation for Fracturing 23
3.1.2. Synthetic Fracture Fabrication 26
3.2. Experimental Set-up 30
3.2.1. Apparatus 30
3.2.2. Fluid Flow through Fracture 33
3.3. Fracture Plane Characterization 35
3.3.1. Hydraulic Tests 35
3.3.2. Tracer Tests 36
3.4. DNAPL Entrapment 40
3.4.1. Materials 40
3.4.2. Apparatus 41
3.4.3. Methodology 43
3.5. Interfacial Tracer Tests 45
3.5.1. Materials 46
3.5.2. Interfacial Tracer Experiments 47
3.5.3. Interfacial Tension Measurement 50
3.5.4. Interfacial Area –Photo Analysis 50

CHAPTER 4: RESULTS AND DISCUSSION 53
4.1 Fracture Plane Characterization 53
4.1.1. Hydraulic Studies 54

TABLE OF CONTENTS

Page

4.1.2. Tracer Studies..... 58
4.1.3. Fracture Volume Determination..... 64
4.2. DNAPL Entrapment..... 64
4.3. Interfacial Tracer Tests..... 70
4.3.1. Interfacial Tracer Distribution Coefficient, K_i 70
4.3.2. Background Sorption of SDBS..... 73
4.3.3. Tracer Breakthrough Curves..... 74
4.3.4. Specific DNAPL-Water Interfacial Area, a_{nw} 78
4.3.5. Verification of a_{nw} Through Visualization..... 80
4.3.6. Possible Reasons for the Small Discrepancies..... 81

5.0 CHAPTER 5: CONCLUSIONS..... 86
5.1. Aperture Field Characterization..... 86
5.2. DNAPL Entrapment Experiments..... 86
5.3. Interfacial Tracer Technique..... 87
5.4. Specific DNAPL-Water Interfacial Area, a_{nw} 88
5.5. Verification of the Experimental a_{nw}..... 90
5.6. Recommendations..... 91

6.0 REFERENCES..... 93

APPENDIX A: Calibration Data..... 98
APPENDIX B: Interfacial Tension Data..... 100
APPENDIX C: Tracer Experiments' Data..... 103
APPENDIX D: Interfacial Tracer Experiments' Data..... 105

LIST OF FIGURES

Figure 2-1: A cartoon of surfactant molecules adsorbed in a monolayer at the interface between a DNAPL blob and water..... 15

Figure 2-2: A plot of the interfacial tension (γ) between a surfactant and a typical DNAPL against the log of dilute surfactant concentrations (C) (after Rosen, 1978)..... 16

Figure 3-1: The granite sample was taken from this outcrop along Highway 118 just west of Carnarvon, Ontario..... 24

Figure 3-2: A student cutting the granite rock using the Quick Cut saw..... 24

Figure 3-3: Diagram of sample prepared for the induction of a fracture..... 25

Figure 3-4: Figure of the FRP wrapped around rock cube..... 26

Figure 3-5: Schematic diagram of the casting process (modified from Dickson, 2001)..... 27

Figure 3-6: Open faces of granite rock fracture..... 28

Figure 3-7: Rubber moulds of fracture planes with wooden plates removed (note: the scale is in inches)..... 29

Figure 3-8: Mated epoxy halves, forming the transparent cast of the granite rock fracture (note: the scale is in inches)..... 29

Figure 3-9: A schematic of the re-circulation system..... 32

Figure 3.10: A schematic of the experimental apparatus for water flow through the cast..... 34

Figure 3-11: Schematic of acid yellow 17 tracer test..... 38

Figure 3-12: A schematic diagram of the experimental apparatus. Note that the red colour represents the DNAPL..... 42

Figure 3-13: The chemical structure of the sodium salt of dodecylbenzene-sulfonate (SDBS) used in the interfacial tracer tests..... 46

Figure 3-14: A side-view photo of red-dyed water flowing through the fracture cast with HFE7100 entrapped (seen as the colourless phase)..... 51

Figure 4-1a: Head loss across fracture 1 in response to specific discharge (q) and Reynolds Number (Re). The q calculation was based on e_h, where $q = Q/We_h$. The linear relationship had an R^2 of 0.988. The Re was calculated using (4-2). The error bars were estimated based on the measurement error in head loss and flow readings..... 57

Figure 4-1b: Head loss across fracture 2 in response to specific discharge (q) and Reynolds Number (Re). The q calculation was based on e_h, where $q = Q/We_h$. The linear relationship had an R^2 of 0.9006. The Re was calculated using (4-2). The error bars were estimated based on the measurement error in head loss and flow readings..... 58

Figure 4-2a: Breakthrough curve for acid yellow 17 in fracture 1. Note the influent concentration took some time to reach unity, therefore for the average influent concentration for 0-114 minutes was used to normalize the effluent concentrations in this time period, and the overall average influent concentration was used to normalize the remaining effluent concentrations. These influent averages were selected to best represent the average influent concentration for these specific time periods..... 61

Figure 4-2b: Breakthrough curve for acid yellow 17 in fracture 2. Note that no average influent concentration adjustments were necessary here since the influent concentration reach unity relatively quickly..... 62

Figure 4-3a: Plan view of the HFE7100 entrapped in fracture 1, experiment 1. The HFE7100 is represented by the colourless liquid, while the aqueous phase has been dyed red (as seen as the dark grey colour). 68

Figure 4-3b: Plan view of the HFE7100 entrapped in fracture 1 inclined at a 20° angle, experiment 2. The HFE7100 is represented by the colourless liquid, while the aqueous phase has been dyed red (as seen as the dark grey colour). 69

Figure 4-3c: Plan view of the HFE7100 entrapped in fracture 2, experiment 3. The HFE7100 is represented by the colourless liquid, while the aqueous phase has been dyed red (as seen as the dark grey colour). Note the large pinkish-white blob in the upper right corner of the picture is the upper boundary of the fracture plane, not a HFE7100 blob..... 69

Figure 4-4a: Interfacial tension measured at various HFE7100-SDBS solution interfaces for SDBS solutions between 0-120 mg/L.....72

Figure 4-4b: Natural log plot of interfacial tension measured at various HFE7100-SDBS solution interfaces for SDBS solutions between 0-120 mg/L..... 72

Figure 4-5a: BTCs for SDBS (reactive) and acid yellow 17 (non-reactive) tracers in fracture 1 experiment 1..... 77

Figure 4-5b: BTCs for SDBS (reactive) and acid yellow 17 (non-reactive) tracers in fracture 1 experiment 2. 77

Figure 4-5c: BTCs for SDBS (reactive) and acid yellow 17 (non-reactive) tracers in fracture 2 experiment 3..... 78

Figure 4-6a: Tracer flow (arrows) that by-passes small HFE7100 blobs (grey patches) along the flow path..... 82

Figure 4-6b: Tracer flow (arrow) impeded by large asperities along the fracture plane, thereby preventing contact with the HFE7100 blob trapped behind asperity (grey patch)..... 82

LIST OF TABLES

Table 3-1: Volume of re-circulation system for the fracture casts..... 37

Table 4-1a: Three apertures calculated for the same valid specific discharge, q range. Note that W (perpendicular to flow) and L (parallel to flow) refer to the fracture width and length respectively..... 56

Table 4-1b: Actual apertures calculated for the valid q range and the valid t_m values..... 58

Table 4-2: Fracture volumes based on the mass balance aperture calculation...64

Table 4-3: Summary of the experimental conditions and results for the HFE7100 Entrapment Experiments..... 65

Table 4-4: Summary of regression fits to interfacial tension data for three DNAPL-SDBS solution plots (source: current Fisher Scientific MSDS sheets)..... 73

Table 4-5: Summary of parameters for interfacial tracer experiments.....79

Table 4-6: Summary of interfacial areas obtained using the digital image software and compared to the experimental interfacial areas.....80

CHAPTER 1: INTRODUCTION

Many contaminants exist in the subsurface, threatening the integrity of the groundwater that many people, including 25-30% of Canadians, rely on as a potable water supply (Freeze and Cherry, 1979). Some would argue an important class of groundwater contaminants is dense non-aqueous phase liquids (DNAPLs). Typically DNAPLS enter the subsurface from leaky tanks, waste impoundments, and lagoons. Traditionally, it was thought to be ideal to bury waste in impoundments and lagoons that were underlain by rock and clay deposits due to the relatively low permeability of these materials. However, in many cases, those deposits were fractured, which provided excellent pathways for DNAPL migration. Examples of such sites include Smithville Waste Storage Facility in Ontario, Canada and the Bear Creek Burial Grounds Hazardous Waste Disposal Unit in Tennessee, USA (Dickson, 2001).

Because DNAPLs are more dense than water, they tend to sink below the water table in subsurface environments. When a small volume of DNAPL comes into contact with ground water, it has the potential to cause large-scale ground water contamination due to the unique physical properties of this class of compounds. DNAPLs have relatively low viscosities and low aqueous solubilities; once they reach the ground water system, they can migrate over considerable distances, all the while dissolving into the aqueous phase at low concentrations. Although the aqueous solubilities of DNAPLs are relatively low, the drinking water standards set by many regulatory agencies for this class of compounds are typically several orders of magnitude lower (e.g., World Health

Organization, Province of Ontario). Therefore a small volume of DNAPL has the potential to contaminate a large volume of groundwater. For example the maximum allowable concentration of trichloroethylene (TCE) in drinking water in Ontario is 50 ppb (Ontario Regulation 169/03-schedule 2, 2002), and the World Health Organization suggests 70 ppb (WHO, 1996). Therefore, taking 50 ppb as the maximum allowable concentration, 1 litre of TCE could potentially contaminate 29 million litres of groundwater.

Once released into the subsurface, DNAPLs migrate according to the forces acting on the system. A DNAPL mass will continue to migrate in a forward direction under the influence of gravitational and viscous forces, while capillary forces hinder the forward movement. A portion of the DNAPL mass becomes entrapped and is rendered immobile when the capillary forces exceed the gravitational and viscous forces. The entrapped DNAPL mass acts as a long-term source zone for groundwater contamination since the DNAPL slowly dissolves into the aqueous phase over time. As a result, DNAPLs are considered to be an enduring threat to groundwater quality.

DNAPL site investigations require a good understanding of the hydrologic and hydrodynamic properties of the site, as well as the origin of contamination and the methods of migration through the subsurface. This information, together with an accurate characterization of the DNAPL source zone, enables investigators to assess the risk to human and ecological health, select an effective remediation technique, or develop a

suitable monitoring strategy. Accurate source zone characterization involves delineating the distribution, volume, and compositional nature of DNAPL waste present.

Because of the typically complex distribution of DNAPL source zones, traditional point measurement techniques (e.g. core sampling, cone penetrometer testing, and geophysical logging) used in unconsolidated porous media provide uncertain estimations of the true mass of DNAPL trapped (Willson et al., 2000), particularly in heterogeneous environments such as fractured rock. It has been suggested that tracer techniques may be both more reliable and cost-effective than these traditional methods used in unconsolidated porous media environments (Annable, 1998a). There are many advantages to tracer techniques including: they are non-invasive, they do not require a description of the solid geometry, and they sample a larger volume of the contaminated aquifer. Additionally, tracer techniques have the potential to be far more cost effective than traditional point measurement techniques. Together, these attributes make the tracer test ideal for characterizing DNAPL source zones in fractured rock at the field scale.

Two different tracer techniques have been used to characterize DNAPL source zones: the partitioning tracer technique, which measures the DNAPL saturation, S_N and the interfacial tracer technique, which measures the DNAPL-water interfacial area, a_{nw}. The DNAPL-water interfacial area is important, as it is a measure of the surface area available for mass transfer, which determines the length of time the trapped mass will persist without remedial intervention. Additionally, many remediation techniques are

based on the mass transfer mechanism (e.g., pump and treat, soil vapour extraction). Both the DNAPL-water interfacial area and the DNAPL saturation are important parameters, as the ratio of these parameters represents the DNAPL morphology, H_N. The morphology provides a measure of the geometry and spatial distribution of the DNAPL trapped in the fracture plane (Annable et al., 1998a), which is an important factor to consider when developing a monitoring or remediation strategy. Although these tracer techniques have shown promise for accurate DNAPL source zone characterization in unconsolidated porous media, they have yet to be applied to fractured rock environments.

1.1. RESEARCH GOAL AND OBJECTIVES

The goal of this research was to develop the interfacial tracer technique for fractured rock environments. The goal of this research was met through the following objectives:

- A transparent cast of a granite fracture was fabricated. This cast, along with a cast of a limestone fracture prepared by Dickson (2001), were employed to visually observe entrapped DNAPL geometries, and directly measure the fluid-fluid interfacial areas. Additionally, they enabled the comparison of DNAPL behaviour in two unique aperture fields, existing in two different rock types.
- Both fracture casts were characterized using hydraulic and tracer techniques to characterize the effective aperture.
- The interfacial tracer technique was developed for fractured rock systems, and was tested and calibrated in both fracture casts. Values for the DNAPL-water interfacial area were obtained.

- The experimental interfacial area results were verified against those obtained through an image analysis of the fluid-fluid interfacial area using Image Tool software (UTHSCSA, version 3.00).

This thesis contains 4 additional chapters: Chapter 2 provides background information on the principles governing two-phase flow and DNAPL entrapment in subsurface environments, and discusses the interfacial tracer technique employed in porous media environments; Chapter 3 describes the experimental materials, methods and design employed in this work; Chapter 4 presents the experimental results and discusses the implications of these results; and Chapter 5 presents the conclusions and provides recommendations for future work.

CHAPTER 2: BACKGROUND

A number of studies have successfully characterized DNAPL source zones in porous media using several parameters, including the DNAPL-water interfacial area, a_{nw}. However, very few studies have focused on DNAPL source zone characterization in fractured rock systems. Two key areas of study that relate to DNAPL source zone characterization are: the principles governing two-phase flow and the mechanisms controlling DNAPL entrapment. Both these areas of study are well understood in porous media environments, however fewer studies have been conducted in fractured media environments. Kueper and MCWhorter (1991) postulated that the distribution of asperities in rough-walled fractures parallels the distribution of pore space in unconsolidated porous media; therefore, the literature generated by the porous media field may be instructive towards the understanding of fractured rock systems.

Because the fractured rock environment is often described using theories and principles developed for the porous media system, it is possible that the methods used to characterize DNAPL trapped in porous media can also be applied to fractured rock environments. Interfacial tracer techniques (IFTT) have recently been developed for porous media environments, to measure the interfacial area between the DNAPL source zone and surrounding aqueous phase. Although this method has been successful in both lab and field experiments in porous media, no research has been done to determine its applicability to fractured rock systems.

The following sections describe the general principles that govern two-phase flow and DNAPL entrapment in fractured rock, present the theory behind the IFTT, discuss field and laboratory investigations concerning the IFTT, and consider the potential shortcomings of the IFTT method. The body of literature in the following sections is comprised of that generated by the environmental and hydrogeological fields.

2.1 THE FORCES GOVERNING DNAPL MOVEMENT

Because the variations in asperities along a fracture plane mimic the variations in pore sizes existing in porous media, the forces governing DNAPL movement in porous media are the same as those found in fractured media: capillary, viscous and gravitational forces. A DNAPL mass will migrate through a fracture plane in a forward direction under the influence of gravitational and viscous forces, while capillary forces act to resist the forward movement.

2.1.1. Capillary Force

Capillary pressure is the pressure difference across the interface between two immiscible fluids due to the interfacial tension between the two fluids. Capillary pressure is responsible for opposing the forward movement of a DNAPL mass. The magnitude of capillary pressure is dependent on the size of the pore space; the smaller the pore is, the larger the capillary pressure will be. In fractured environments, pore spaces are represented by aperture widths. The capillary pressure across a DNAPL-water interface

trapped in a fractured rock can be described by the Laplace equation for equilibrium capillary pressure (Dullien, 1979):

$$\Delta P_c = P_{nw} - P_w = \sigma_{wn}\left[\frac{1}{r_u} + \frac{1}{r_d}\right] \tag{2-1}$$

where ΔP_c [$M \cdot L^{-1} \cdot T^{-2}$] represents the capillary pressure drop across the interface between two fluids, P_{nw} [$M \cdot L^{-1} \cdot T^{-2}$] represents the pressure in the non-wetting fluid (DNAPL), P_w [$M \cdot L^{-1} \cdot T^{-2}$] represents the pressure in the wetting fluid (water), σ_{wn} [$M \cdot T^{-2}$] represents the interfacial tension between the wetting and non-wetting phases, and r_u [L] and r_d [L] represent the upstream and downstream radii of curvature of the interfacial boundary respectively. It is customary to combine the radii of curvature into a mean radius of curvature, r_m [L], defined by (Dullien, 1979):

$$\frac{1}{r_m} = \frac{1}{2}\left(\frac{1}{r_u} + \frac{1}{r_d}\right) \tag{2-2}$$

Incorporating both the mean radius of curvature and the geometry of the meniscus into the Laplace equation gives (Dullien, 1979):

$$\Delta P_c = \frac{2\sigma\cos(\theta)}{r_m} \tag{2-3}$$

where θ [degrees] represents the contact angle between the two fluids with respect to the solid surface.

2.1.2. Viscous Force

Viscous forces are caused by water flowing around a trapped DNAPL mass, which acts to mobilize that mass. Dickson (2001) defines the pressure drop due to viscous forces across the length of a trapped DNAPL mass, assuming horizontal flow and neglecting relative permeability:

$$\Delta P_v = \frac{v_w V_w L_H}{k} \tag{2-4}$$

where ΔP_v [M·L^{-1}·T^{-2}] represents the viscous pressure drop across the horizontal DNAPL length, L_H [L] is the horizontal length of the DNAPL mass, v_w [M·L^{-1}·T^{-2}] is the dynamic viscosity of the wetting phase, V_w [L·T^{-2}] is the wetting phase velocity, and k [L^2] is the intrinsic permeability of the medium.

2.1.3. Gravitational Force

When non-horizontal flow exits, the density difference between the wetting and non-wetting fluids causes a gravity or buoyant force that tends to mobilize the entrapped DNAPL mass. The gravity pressure drop (ΔP_g) across an entrapped mass is expressed as (Dickson, 2001):

$$\Delta P_g = (\rho_n - \rho_w) g L_v \tag{2-5}$$

where ρ_n and ρ_w [M·L^{-3}] are the non-wetting and wetting phase densities respectively, g [L·T^{-2}] is the acceleration due to gravity, and L_v [L] is the vertical length of the DNAPL mass.

2.2. DNAPL MIGRATION IN FRACTURES

In order for a DNAPL mass to enter small aperture regions within a fracture plane, the capillary pressure at the edge of the DNAPL mass must exceed the entry pressure of the aperture region. Assuming that the void space into which the DNAPL is about to enter takes the shape of two parallel plates, the entry pressure is (Kueper and McWhorter, 1991):

$$P_e = \frac{2\sigma \cos\theta}{e} \tag{2-6}$$

where P_e [M·L^{-1}·T^{-2}] is the entry pressure, and e [L] is the aperture width. However, if the void space is circular in shape, then the entry pressure is (Kueper and McWhorter, 1991):

$$P_e = \frac{4\sigma \cos\theta}{e} \tag{2-7}$$

where e [L] is the diameter of the void space.

In reality, entry pressure values in fractures lie somewhere between (2-6) and (2-7), because fracture planes are typically rough-walled, and the void space geometry is irregular. In fact, Kueper and McWhorter (1991) postulate that the actual entry pressure of a fracture will most likely approach that given by (2-6) since the DNAPL-water interface is likely to be elongated in the direction of the fracture plane.

2.3 DNAPL ENTRAPMENT

A portion of the DNAPL mass becomes entrapped and is rendered immobile when the capillary forces exceed the gravitational and viscous forces. The size and shape of the entrapped DNAPL depends on the geometry of the pore/aperture openings, the fluid-fluid properties (interfacial tension, and viscosity and density of the fluids), the fluid-solid properties (wettability), and the external forces on the fluids (pressure gradients and gravity) (Dickson, 2001). The characteristics of the DNAPL source zone are important; they include the DNAPL-water interfacial area, the entrapped DNAPL volume, the location of the DNAPL source zone, and the type of DNAPL present.

The ratio of the fluid-fluid interfacial area to volume of trapped DNAPL, often referred to as the morphology, is an important factor in determining mass transfer rates to the surrounding aqueous phase. The morphology index is an important parameter, as it provides an index of the entrapped DNAPL distribution. Because the configuration of trapped DNAPL has significant implications for the mass transfer process, the morphology index plays a key role in the rate of mass transfer that can be achieved. It is the mass transfer rate that determines the length of time that a DNAPL source zone will persist in the absence of remedial intervention. Additionally, the efficiency of many remediation technologies is dependent on the mass transfer rate.

2.3.1. Stability Measures for Entrapped DNAPL Mass

A number of dimensionless correlations exist in the literature to provide a measure of the potential for a DNAPL mass to migrate. In the case of horizontal flow, where gravitational forces are negligible, an appropriate stability measure is the capillary number, defined as the ratio of mobilizing viscous forces to resistive capillary forces. In a fractured rock system, when the two phases are immiscible, the capillary number, and can be expressed as:

$$N_c = \frac{\mu v}{\sigma \cos\theta} = \frac{k \rho_w g \nabla H}{\sigma \cos\theta} \tag{2-8}$$

where N_c [-] represents the capillary number, μ [$L \cdot T^{-1}$] is the linear velocity based the Darcy flux, v [$M \cdot L^{-1} \cdot T^{-2}$] is the dynamic viscosity of the wetting phase, ρ_w [M/L^3] is the density of water, g [M/T^2] is the gravitation constant, ∇H [-] is the hydraulic gradient, σ [M/T^2] is the fluid-fluid interfacial tension, θ [degrees] is the wetting contact angle, k [L^2] is the fracture intrinsic permeability and is calculated as: $k = e_h^2/12$, where e_h [L] is an equivalent aperture.

2.4. INTERFACIAL TRACER TECHNIQUE

Accurate characterization of DNAPL source zones requires understanding the hydrologic and hydrodynamic conditions at the site, delineating the distribution, volume, and compositional nature of DNAPL, and measuring fluid saturations and specific interfacial areas. Of late, researchers have begun to recognize the fluid-fluid interfacial area, a_{nw} [$L^2 \cdot L^{-3}$] as a fundamental variable necessary to describe the status of

immiscible fluids in soils and aquifers. In earlier studies, researchers have relied on theoretical estimates of a_{nw} that could not be validated by direct measurements (Gvirtzmann and Roberts, 1991; Powers et al., 1991; Reeves and Celia, 1996). More recently, however, Saripalli et al. (1997a) have reported an experimental method to measure a_{nw} using interfacial tracers, which has been successful in several unconsolidated porous media studies (Saripalli et al., 1997b, Annable et al., 1998a; Kim et al., 1997). The a_{nw} variable is an important property for DNAPL source zone characterization as it represents the surface area available for mass transfer processes. The following section describes the interfacial tracer technique developed for porous media environments for the purposes of calculating the a_{nw} parameter.

2.4.1. The Interfacial Tracer Technique –An Overview

The experimental approach using interfacial tracers for estimating the interfacial area between two immiscible fluids, a_{nw} involves displacing a pulse or step input of tracers (non-reactive and reactive) through the test zone under steady state conditions, and measuring the retardation of the reactive tracer with respect to the non-reactive tracer. The reactive tracer is retarded because it adsorbs to the interface between the two immiscible fluids, without significantly adsorbing to the solid matrix or any other phases present, while the non-reactive tracer does not adsorb to any interface. During displacement, the non-reactive and reactive tracers experience the same hydrodynamic conditions, but the average travel time for the reactive tracer is delayed due to the specific interactions with the DNAPL.

The chromatographic separation between the reactive and non-reactive tracer breakthrough curves is used to determine the retardation factor, which corresponds to an interfacial area between the non-aqueous and aqueous phases. Tracer travel times are typically determined by moment analysis of tracer breakthrough curves for each sampling location.

2.4.2. Surfactant Adsorption at the DNAPL-Water Interface

Interfacial tracers are surface-active agents that have the unique chemical property to adsorb at the interface between two immiscible fluids (DNAPL and water), without partitioning into the immiscible phase (DNAPL). The degree of interfacial tracer adsorption is dependant mostly on its hydrophilic-hydrophobic balance, and on the nature of the fluids in the system as well as the thermodynamic conditions present (Kim et al, 1999). The surfactant selected as the interfacial tracer should not adsorb to the solid matrix or any other phases except the fluid-fluid interface of interest.

Anionic and cationic surfactants and high molecular-weight alcohols are used as interfacial tracers as they have been successful at adsorbing in monolayers at the fluid-fluid interface only (Saripalli et al., 1998, Kim et al., 1999; Rao et al., 1998). These surfactants consist of a hydrophobic chain and a hydrophilic head, where the chain is commonly an alkyl linear or branched chain, and the head is ionic or highly polar. Adsorptive power is largely increased when the number of carbons in the alkyl chain is increased and when a benzene ring is present (Healy et al., 2003).

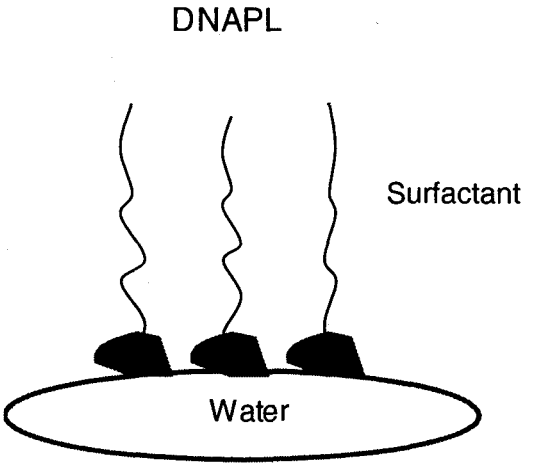

Figure 2-1: A cartoon of surfactant molecules adsorbed in a monolayer at the interface between a DNAPL blob and water.

Monomers of surfactants readily adsorb at the interface between two immiscible fluids. The interface is a thin layer, which acts as a stretched membrane of infinitesimal thickness and is subject to interfacial tension due to the intermolecular forces of each fluid (Dullien, 1979). Because the immiscible fluids have different properties, they exert unbalanced forces that cause the interface to seek a state of minimum excess free energy or minimum surface area, resulting in a curved interface (Dullien, 1979).

As long as the surfactant remains in monomeric form, it will continue to adsorb at the DNAPL-water interface, without influencing the interfacial tension. Any change in the interfacial tension would be problematic as it could result in altered DNAPL saturations and fluid-fluid interfacial areas. To ensure that the surfactant remains in monomeric form throughout the tracer experiments, the surfactant concentration should

be less than its critical micelle concentration (CMC). The CMC is the concentration at which the surfactant adsorption is saturated; at this point the surfactant no longer exists as monomers, rather it exists as aggregates of monomers known as micelles (Figure 2-2) (Rosen, 1978).

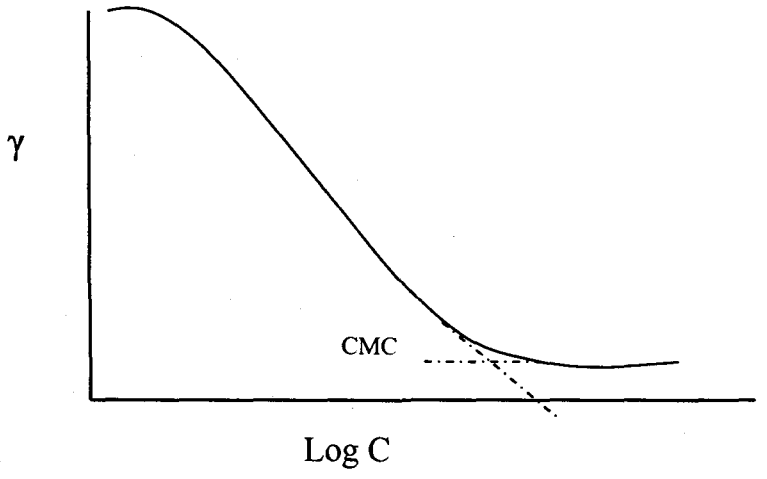

Figure 2-2: A plot of the interfacial tension (γ) between a surfactant and a typical DNAPL against the log of dilute surfactant concentrations (C) (after Rosen, 1978).

Surfactant concentrations below but near the CMC are also considered to be at adsorption saturation since the interfacial tension is essentially constant (Rosen, 1978). Any continued reduction in the interfacial tension, when the surfactant concentration is at or just below the CMC, is mainly due to increased activity of the surfactant in the bulk solution. This may act to enhance dissolution of the residual DNAPL, thus changing the DNAPL morphology and a_{nw} (Saripalli et al., 1998). In general, an initial tracer concentration in the sub-CMC range that lowers interfacial tensions (by approximately 5

dynes/cm) is not considered low enough to mobilize typical DNAPLs and thus is a reasonable concentration choice for maintaining DNAPL morphology and a_{nw} (Saripalli et al., 1998).

Adsorption of surfactant at the fluid-fluid interface is expressed by the Gibbs adsorption equation, which describes the non-linear isotherm representing the accumulation of an interfacial tracer at the fluid-fluid interface:

$$\Gamma = -\frac{1}{2RT}\left(\frac{\partial \gamma}{\partial C}\right)_T C \qquad (2\text{-}9)$$

where Γ [mol·L^{-2}] is the surface excess of surfactant, R [M·L^2·T^{-2}·mol·K] is the ideal gas constant, γ [M·T^{-2}] is the interfacial tension, C [mol·L^{-3}] is the bulk tracer concentration, T [K] is the temperature. It is noteworthy that the application of equation (2-9) requires the assumption that the aqueous solution is dilute (Rosen, 1978).

The Gibbs adsorption equation provides a general thermodynamic approach for describing adsorption using liquid tracers, and is commonly used in the literature for calculating surface concentrations at the immiscible fluid-fluid interface (Saripalli et al., 1997a; Saripalli et al., 1998; Kim et al., 1999; Annable et al., 1998a). It relies on the assumption that the surface excess concentration, Γ, represents the actual concentration adsorbed at the interface, G [mol·L^{-2}]. This is a valid assumption, since Γ can be considered equal to the mass adsorbed per unit interfacial area obtained experimentally without significant error (Rosen, 1978). However, Saripalli et al. (1998) noted that there

is a subtle difference between the thermodynamic entity, Γ, and the experimentally measured value, G.

Because the interfacial adsorption isotherm for a surfactant is a strong non-linear function of the bulk concentration for most fluid-fluid interfaces, it is important to utilize an interfacial adsorption coefficient, K_i, which optimally represents the distribution characteristics of the tracer between the bulk phase at the fluid-fluid interface. For a step tracer input, the simplest method is to use the adsorption distribution relation (G_o/ C_o) at the initial surfactant concentration, C_o:

$$K_i = \frac{G_o}{C_o} = -\frac{1}{2RT}\left(\frac{\partial \gamma}{\partial C}\right)_{C_o,T} \tag{2-10}$$

where G_o [L] and K_i [M/L^2] are the surface excess and adsorption coefficients respectively at an initial tracer concentration, C_o [M/L^3] (Kim et al., 1999; Saripalli et al., 1998). Recall that R [M·L^2·T^{-2}·mol·temp] is the ideal gas constant, γ [M·T^{-2}] is the interfacial tension, C [mol·L^{-3}] is the bulk tracer concentration, and T [K] is the temperature. The estimation of the retardation factor from the breakthrough curve with a continuous step-input of interfacial tracers is described in the following section.

2.4.3. Retardation Model & Interfacial Area Calculation

The retardation factor describes the difference in interfacial tracer transport relative to the non-reactive tracer, which is defined from advection-dispersion theory of reactive solute transport through porous media, assuming that the interfacial tracer only

adsorbs at the fluid-fluid interface. The retardation factor, R_{ift} [-], relies on a rather complicated equation since the relation between tracer retardation and interfacial area are difficult to determine independently; it is defined as (Saripalli et al., 1998; Saripalli et al, 1997a):

$$R_{ift} = \frac{\mu_{ift}}{\mu_{nr}} = 1 + \frac{a_{nw} K_i}{\theta_w} \tag{2-11}$$

where μ [T] is the area above the breakthrough curve measured for a continuous (or step) tracer input for the interfacial and non-reactive tracers labelled $_{ift}$ and $_{nr}$ respectively. μ is given by (Saripalli et al., 1998):

$$\mu = \int_0^\infty (1 - C^*(t))dt \tag{2-12}$$

and $C^*(t)$ [-] = $C(t)$ [M·L^{-3}] / C_o [M·L^{-3}] is the normalized concentration of the tracer of interest, C_o [M·L^{-3}] is the influent tracer concentration, θ_w [-] is the volumetric water content, K_i [-] is the interfacial adsorption distribution coefficient, and a_{nw} [L^2·L^{-3}] is the DNAPL-water interfacial area, expressed as the interfacial area per volume of the system. For step tracer input experiments, assuming no solid phase adsorption, a_{nw}, can be estimated by (Saripalli et al., 1998):

$$a_{nw} = \frac{(R_{ift} - 1)\theta_w}{K_i} \tag{2-13}$$

2.4.4. Reliability of the Retardation Model

In general, the displacement experiments rely on the assumption that the entire DNAPL phase is in contact with the aqueous phase. In some cases, the tracer technique may underestimate a_{nw} if some of the DNAPL-water area is somehow isolated from the mobile aqueous phase in which the tracers are being transported. Similarly, highly heterogeneous distribution of the DNAPL and heterogeneous systems such as variable aperture fractures can present additional challenges in data interpretation and introduce significant uncertainties.

In heterogeneous systems such as fractured rock, asymmetric tracer breakthrough curves may result due to the spatial heterogeneities of the variable aperture fracture, the spatial distribution of DNAPL, and nonequilibrium tracer adsorption at the DNAPL-water interface. Extensive tailing of the breakthrough curve is attributed to nonlinear tracer adsorption (Annable et al., 1998c). A substantial portion of the tail can be below analytical detection and quantification limits. If this 'lost' tracer mass is not included in the moment analysis, the first temporal moment for the curve will be erroneously small and the resultant saturation or interfacial area estimate will be incorrect. In this situation, several studies extrapolate the curves to "zero concentration" by fitting an exponential function to the final portions of the BTC (Cain et al., 2000; Annable et al., 1998c). In some cases, the breakthrough curve tailings may not be adequately fit with a simple log-linear function. Some studies use numerical models to estimate the tracer travel times and solute concentrations at late times (Jin et al., 1997).

There is also some question as to whether the interfacial area, a_{nw} calculation is reliable since the Gibbs adsorption isotherm, Γ is obtained using an a_{nw} value estimated from the K_i value (which is calculated using the Gibbs adsorption equation). Therefore the Gibbs adsorption isotherm, Γ is not completely independent of the γ-C data (Kim et al.,1999). However, Kim and associates (1999) provided a study that tested the Γ dependence on the γ-C data, by comparing the tracer adsorption isotherm based on column displacement experiments, with that predicted by adsorption equation; they found that the interfacial tension measurements are acceptable for determining the interfacial adsorption isotherm and for estimating adsorption coefficients.

In addition, several studies have validated the retardation model by comparing the relationship between tracer retardation and interfacial area to values calculated based on geometrical, thermodynamic considerations, or soil core sampling data (Noordman et al., 2000; Jawitz et al, 2000; Annable et al., 1998a). Nevertheless, a systematic study has not been conducted to determine whether this relation holds for DNAPLs present in various subsurface environments, in particular in fractured rock systems, and at different surface area to volume ratios (Noodman et al., 2000). Therefore more rigorous studies are required to increase the reliability of the retardation model.

CHAPTER 3: EXPERIMENTAL DESIGN

An experiment was designed, based on information available in the porous media literature to develop an interfacial tracer technique for fractured rock systems. The experiment was conducted in transparent replicas of two discrete fractures of different rock types: one granite, the other limestone. Synthetic replicas of these rock fractures were employed in order to visualize DNAPL entry and entrapment in the water-saturated fracture plane. Once the DNAPL was trapped in the fracture plane, the interfacial tracer test was performed in an effort to determine the DNAPL-water interfacial area. The results of these experiments were calibrated and verified using digital photo analysis. This chapter describes the methodology used to prepare the synthetic rock fractures, the experimental apparatus designed to mimic the natural water-saturated fractured rock system, the tests used to characterize the fracture planes, and the details of the interfacial tracer test and digital photo analysis.

3.1 FRACTURE PLANE PREPARATION

Granite rock samples that displayed a plane of weakness were collected from the field and returned to the lab, where tension uni-axial fractures were induced. A transparent epoxy cast of one of the granite rock fractures was fabricated, and used along with a cast of a limestone rock fracture prepared by Dickson (2001). The epoxy casts were necessary for observing two-phase flow along the fracture plane, and for digital

photo analysis of the fluid-fluid interfacial area. The methodologies used to fracture the rocks and fabricate the epoxy fracture plane are described in this section.

3.1.1. Rock Sample Preparation for Fracturing

The granite rock samples were selected from outcrops along Highway 118 just west of Carnarvon, Ontario (Figure 3-1). Each rock sample was chosen because it had a single plane of weakness, such as a change in mineralogy or a styolite, which was ideal for inducing fractures in the lab. The samples were cut from the outcrops (Figure 3-2) using a Quick-Cut saw equipped with a diamond tipped blade and brought to the laboratory.

The rocks were fractured using a methodology adapted from Dickson (2001). The rock samples were first cut into a cube shape and a grinder was applied to the rock cube's face to create smooth flat surfaces. Shallow saw cuts were made along the length of the rock-cube on the two opposing sides that were perpendicular to the plane of weakness. The saw cuts were necessary to stabilize the metal triangular bars along the plane of weakness so that the applied load was transferred directly on to this plane (Figure 3-3).

Figure 3-1: The granite sample was taken from this outcrop along Highway 118 just west of Carnarvon, Ontario.

Figure 3-2: A student cutting the granite rock using the Quick Cut saw.

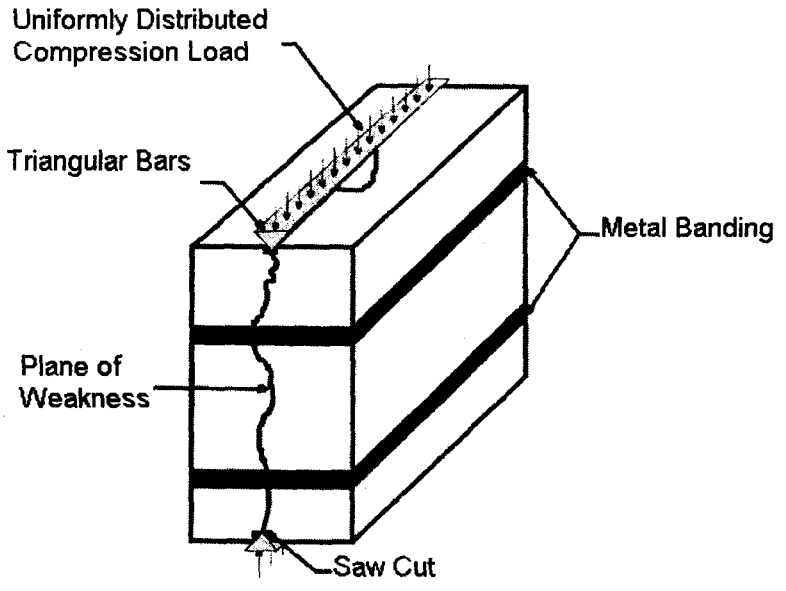

Figure 3-3: Diagram of sample prepared for the induction of a fracture.

The sides of the rock-cube without saw cuts were bound with carbon fibre reinforced polymer (Fyfe Company: Tyfo SCH-35) to secure the rock, so that it only broke along the plane of weakness (Figure 3-4). To further secure the rock's integrity, metal banding was wrapped around each sample, perpendicular to the plane of weakness.

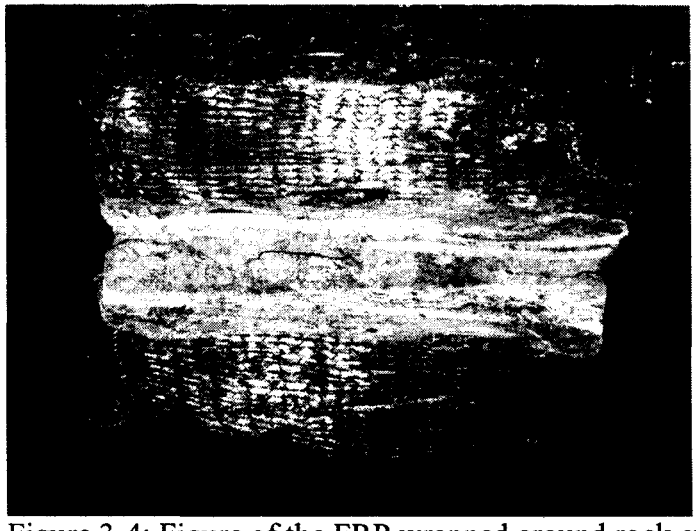

Figure 3-4: Figure of the FRP wrapped around rock cube.

To induce the fracture, the rock-cube, with the triangular bars in place was positioned in a uni-axial compression machine (TINIUS OLSEN universal testing machine, capacity 600kN). A load was applied to the triangular bars, which was directly transferred to the plane of weakness until a tension fracture occurred. This methodology creates tension fractures in a similar manner to those created in nature by compression or stress relief. Once the fracture was created successfully, the metal banding was removed, and the fracture was opened, in preparation for the next stage: fabricating a transparent cast of the fracture plane.

3.1.2 Synthetic Fracture Fabrication

Transparent casts were instrumental for the experiments since they provided a tool for visualizing DNAPL behaviour in fractures. For interest purposes, the DNAPL entry into the fracture plane could be observed in the transparent cast when the water was

dyed red and the DNAPL remained colourless. More importantly however, the transparent cast allowed for the capture of a digital photo of the entrapped DNAPL which was imported into software to calculate the fluid-fluid interfacial area, thereby providing a verification and calibration of the experimental value obtained from the interfacial tracer technique.

The granite rock fracture cast was fabricated using the same method developed by Dickson (2001) employed when fabricating the limestone fracture cast. A general overview of the four-stage process is illustrated in Figure 3-5 and described below.

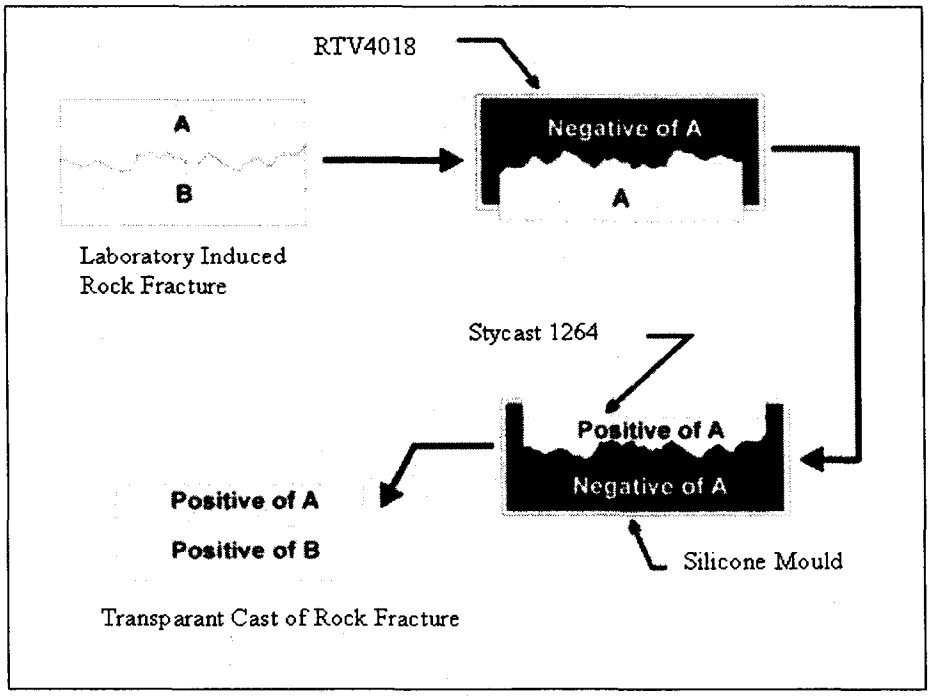

Figure 3-5: Schematic diagram of the casting process (modified from Dickson, 2001).

In stage one, the fracture was induced in the lab, after which the rock was opened along the fracture exposing both faces of the fracture plane (Figure 3-6). The second stage involved constructing a negative mould of the fracture face using liquid rubber made of silicone (RTV-4018, Silchem) (Figure 3-7). Before the silicone negative was removed, a piece of particle board was fixed to the bottom of each mould to prevent any deformation from occurring. The thirds stage, conducted once the silicone cured, involved pouring casting epoxy (Stycast 1264, Emerson Cuming) into the silicone negatives. Finally, once the two epoxy halves were cured, they were mated to complete the synthetic fracture (Figure 3-8).

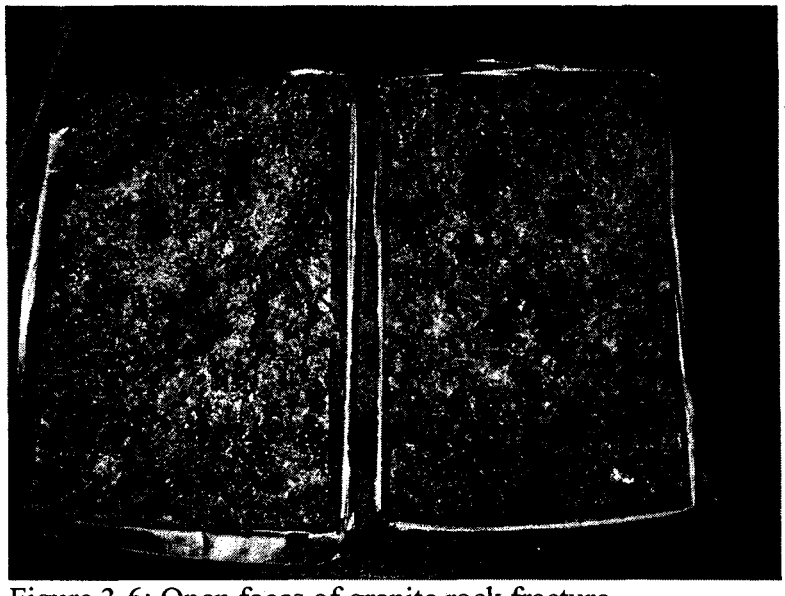

Figure 3-6: Open faces of granite rock fracture.

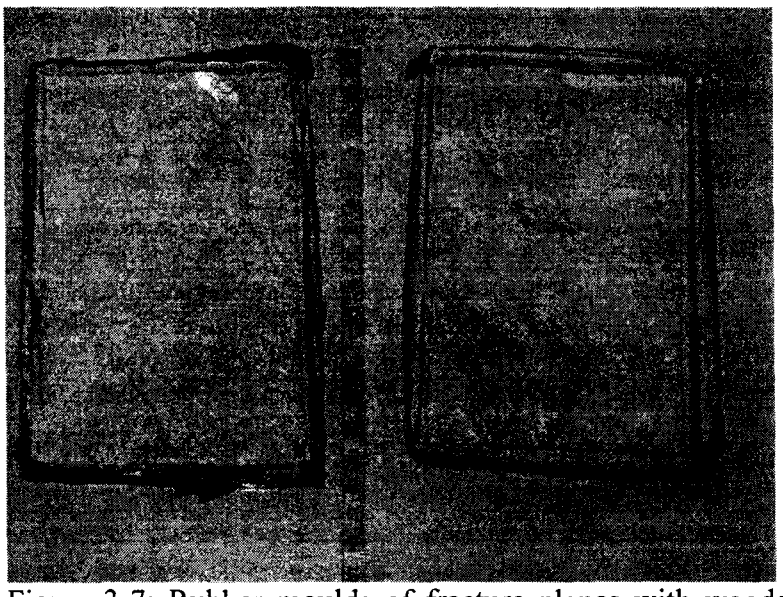

Figure 3-7: Rubber moulds of fracture planes with wooden plates removed (note: the scale is in inches).

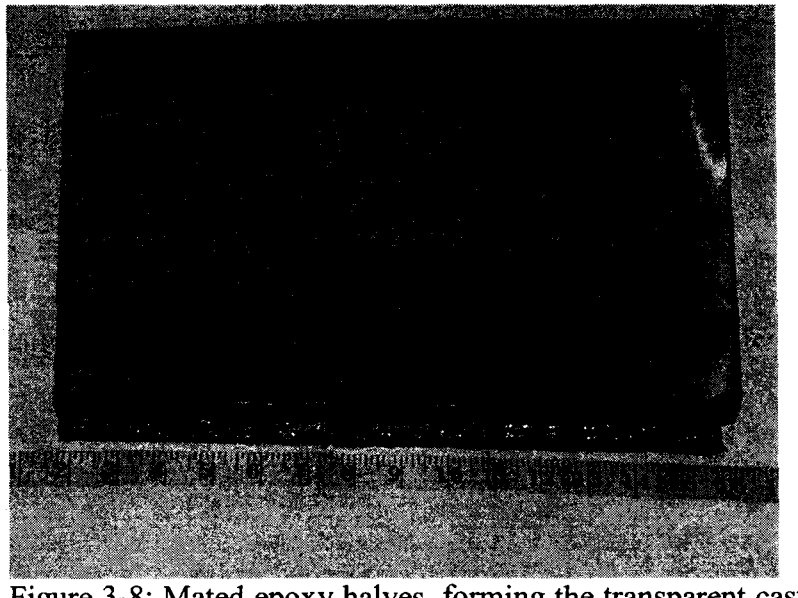

Figure 3-8: Mated epoxy halves, forming the transparent cast of the granite rock fracture (note: the scale is in inches).

The RTV-4018 and Stycast 1264 were ideal materials for the casting process because both had relatively low viscosities, which enabled them to enter into small asperities on the fracture face, thereby providing a good representation of the fracture's

small-scale roughness. The silicone mould was heated to 50°C to enhance the mobility of the epoxy cast, as well as to avoid gas bubble formation during the casting process as recommended by the epoxy manufacturers. Additionally, both the silicone and epoxy were placed under a vacuumed prior to curing to ensure no gas bubbles were trapped.

3.2 EXPERIMENTAL SET-UP

Once the granite fracture cast was complete, both it and the limestone fracture cast were set up in an experimental apparatus designed to mimic a saturated fractured subsurface environment.

3.2.1. Apparatus

Each epoxy fracture plane was fitted with glass end-caps that covered the exposed fracture on the inflow and outflow ends of the fracture. The glass end caps acted as a water reservoir to ensure that the fracture remained saturated during the experiments. The end caps were designed to have three spigots (Figure 3-9). Two of these spigots were located on opposite ends of the end cap, one on the upper side and the other on the lower side. These two spigots were necessary to allow water and other fluids to flow into and out of the fracture. Additionally, because these spigots were located at different elevations, fluid phases could be separated. The third spigot was located at the upper centre of the end-cap where it acted as a manometer. Tygon tubing (Tygon; ID 0.95cm) was attached to the manometer spigots and secured to a metre stick and retort stand so

that measurements of the head loss across the fracture could be taken throughout the experiments (Figure 3-9).

The end-caps were sealed to the fractured cast with silicone (RTV 108, General Electric Company), which provided a flexible joint between two solid materials (glass and epoxy) and allowed for expansion in the case of pressure build up in the system. Stainless Steel putty (ST 10270, Devcon) was used to seal the remaining sides of the epoxy to create no-flow boundaries (Figure 3-10).

A re-circulation system was installed at both the inflow and outflow end-caps to allow for uniform tracer concentrations to be obtained at the inlet and outlet of the fracture plane during the experiments. The re-circulation system (Figure 3-9) was constructed from a piece of Teflon tubing (Tefzel HPLC Tubing, ID 0.130cm) strung through the spigots on either end of the end-cap, through the pieces of Tygon tubing, and through a brass run-t-fitting (Niagara Valve and Fitting: B-200-1-4 and B-400-3TFT). The Teflon tubing inside the end-cap was perforated every 5mm to enable the solution in the end cap to flow freely into and out of the re-circulation tubing. The ends of the Teflon tubing were attached to Masterflex pump tubing (Norprene, ID 0.159cm) to form a complete loop. Within this loop, an 8mL sample vial was inserted for water sampling and injection of tracers. The vial had a screw-cap lid with a hole in the centre for a septum, which allowed for easy sampling and injection using syringes.

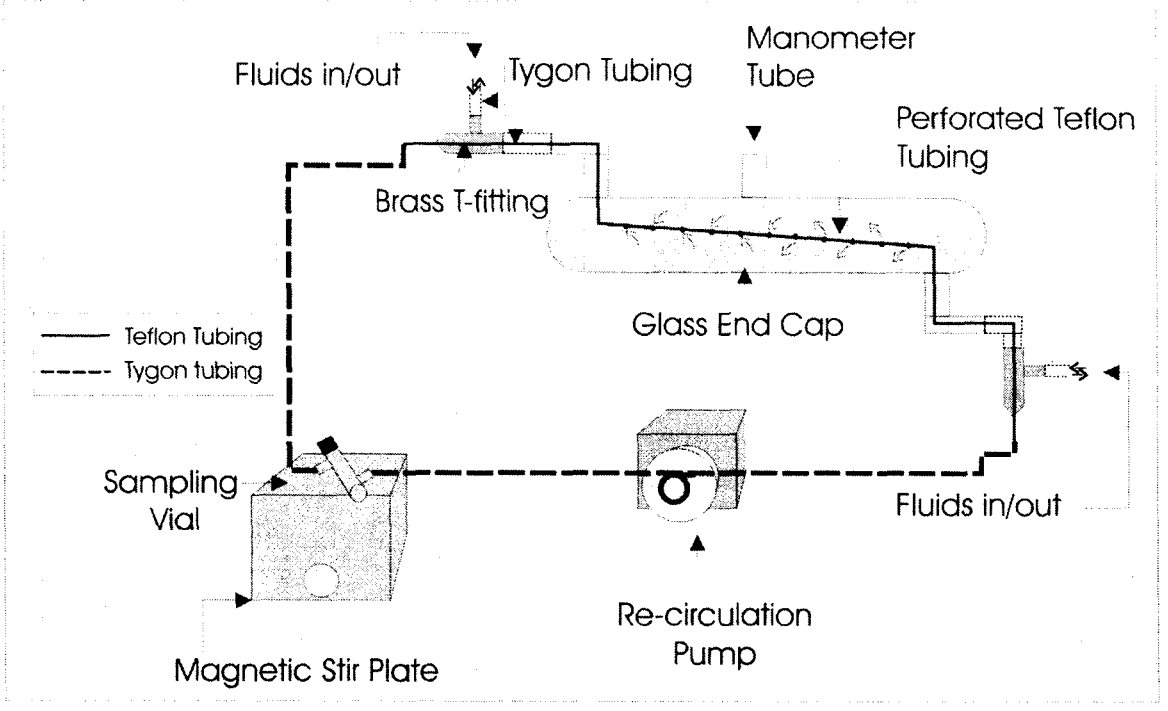

Figure 3-9: A schematic of the re-circulation system.

Throughout the duration of each experiment, a peristaltic pump (Cole-Parmer Instrument Co., 7553-20) was employed to continuously pump the Masterflex tubing, which re-circulated the solution in the end-cap through the perforations in the Teflon tubing. Additionally, the sample vials located within the re-circulation system loop were continuously mixed using a magnetic stir bar and stir plate. This resulted in a uniform solution concentration throughout the re-circulation system, which ensured that the end-cap solution was well represented by the solution in the vial. Table 3-1 provides the volumes of the influent and effluent re-circulation sampling systems for both fracture casts. The run-t-fitting on either spigot of the end-caps allowed for a third connection for fluid flow. Another piece of Teflon tubing was attached to the third arm of the run-t-

fitting, which allowed for the input and withdrawal of fluids to the fractured rock (Figure 3-9).

3.2.2. Fluid Flow through Fracture

Prior to pumping water through the fracture plane, deionised water was degassed under a vacuum, after which the water vessel was sealed with a rubber stopper. The degassed water was then left to equilibrate to room temperature prior to running each experiment. To prepare the fracture for water flow, carbon dioxide was flushed through the fracture cast for approximately 10 minutes to remove any air present in the fracture plane. The degassed water was connected to the fracture inlet and pumped through the system using a peristaltic pump (Cole-Parmer Instrument Co., 7553-20) at a constant rate until the fracture was completely saturated (Figure 3-10). Because carbon dioxide is highly soluble in water, it completely dissolved into the degassed water as it passed through the fracture plane, thereby ensuring no gas pockets were left in the fracture. The water temperature entering the fracture was monitored using a thermister (Lakewood Systems Ltd., TP-10K5) placed in the inflow water storage vessel. This fracture saturation procedure was repeated for all experiments.

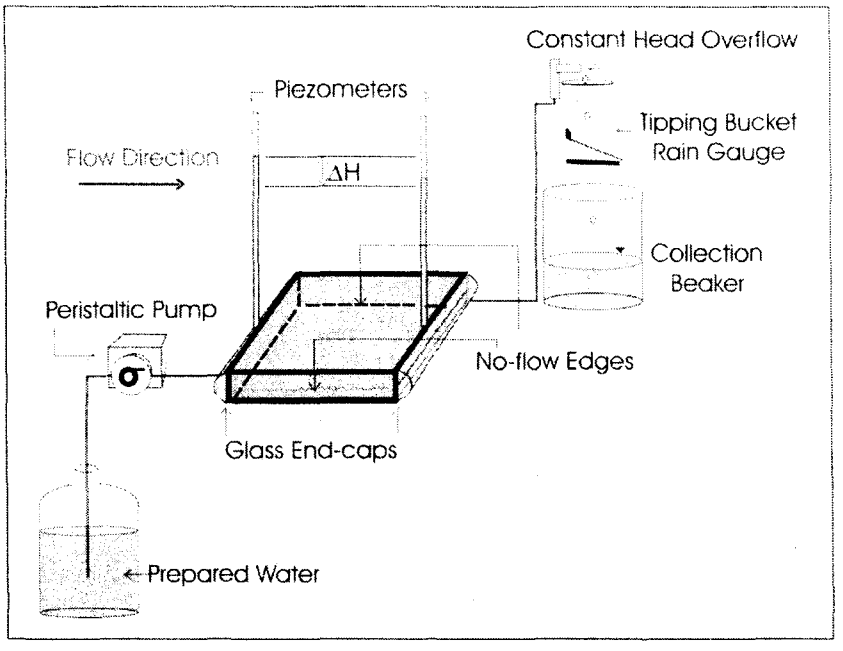

Figure 3.10: A schematic of the experimental apparatus for water flow through the cast.

Water exited the system through the upper spigot of the downstream end cap; the upper spigot was attached to Tygon tubing, which led to a constant head overflow dropper that dripped onto a tipping bucket rain gauge (Davis, Rain Collector II, 7852M), which was used to measure the volumetric flow rate through the system. The rain gauge and thermister were attached to a data logger (Lakewood Systems, Ultra-Logger, UL-16GC), which recorded the number of bucket tips at set time intervals and temperature readings in degrees Celsius. The rain gauge and thermister were calibrated throughout the course of the experiments (Appendix A).

3.3. FRACTURE PLANE CHARACTERIZATION

Both the aperture field and surrounding matrix must be considered when characterizing the fracture plane. In this research, however, the epoxy cast matrix was considered impermeable; therefore it had no influence on fluid flow. As a result, the fracture was characterized by the aperture field only, using both hydraulic and tracer tests.

3.3.1. Hydraulic Tests

For each experiment, when the fracture plane was newly saturated, hydraulic tests were performed to ensure that the equivalent hydraulic aperture had not changed. Using the experimental set-up aforementioned, hydraulic tests were conducted by first saturating the fracture plane, then pumping water through the fracture at a constant flow rate, and measuring the head difference across the fracture plane. The head loss across the fracture plane was measured using a u-tube manometer filled with HFE7100 and water. The head loss was measured in terms of a column of HFE7100 in the u-tube at a given flow rate, and converted to a column of water based on the relative densities of HFE7100 and water at the laboratory temperature.

The known flow rate, head difference and fracture length and width were then used in the cubic law (Snow, 1965) to solve for the hydraulic aperture, e_h, which is defined as the equivalent aperture that satisfies the bulk cubic law (Tsang, 1992). Hydraulic tests were repeated at various flow rates on each fracture plane.

3.3.2. Tracer Tests

Tracer tests, using acid yellow 17 (cas#:6359-98-4, Sigma-Aldrich Canada Ltd.) as the tracer, were performed on each synthetic fracture to determine the mass balance and the frictional loss apertures. The mass balance aperture is a measure of the aperture required to balance a known volume of fluid over the aerial extent of the tracer transport, whereas the frictional loss aperture is based on the mean residence time of the tracer's transport velocity across the fracture plane, assuming that the specific discharge for flow through parallel plates applies to rough-wall fractures (Tsang, 1992).

The tracer test involved four main phases: steady state water flow, tracer release, stepwise tracer input and sampling over time. Water was pumped into the fracture cast at a flow rate equal to that of the interfacial tracer tests. At the same time, a flask of 34 mg/L of acid yellow 17 was prepared. Approximately three times the combined volume of the inflow re-circulation system and end-cap was poured from the flask of acid yellow 17 and set aside. The remaining acid yellow 17 solution was pumped into an empty beaker at the same rate as the water flowing through the fracture in preparation for flow into the fracture.

Table 3-1: Volume of re-circulation system for the fracture casts.

Fracture		End-cap (cm^3)	Re-circulation (cm^3)	Total Volume (cm^3)
Limestone cast (Fracture 1)	Inflow	37.85	20.35	58.20
	Outflow	41.81	15.82	57.63
Granite cast (Fracture 2)	Inflow	189.03	22.15	211.18
	Outflow	161.22	22.35	183.57

Once the cast was completely water-saturated and steady state flow had been reached, the tracer solution was set-up for release into the fracture cast. The volume of acid yellow 17 solution previously set aside was poured into a separatory funnel and the Tygon tubing at the base of the separatory funnel was attached to the third arm of the run-t-fitting at the high spigot of the inflow end-cap and clamped closed. The rubber stopper with the steel pipe was placed into the separatory funnel with the base of the pipe at the same elevation of the outlet spout to ensure constant head. The water flow was stopped, and the acid yellow 17 solution was allowed to pass into the influent end-cap, displacing the existing water, which exited through the lower spigot of the influent end-cap into a beaker. At the same time the re-circulation system was increased to maximum flow to increase the rate of mixing within the influent end-cap.

The acid yellow 17 solution continued to pass through the influent end-cap, at the increased mixing rate for approximately 3 minutes, at which time the acid yellow 17 solution was uniform throughout the influent end-cap and re-circulation/sampling system. At this point, the acid yellow 17 release system was clamped closed, the fracture cast was

re-positioned at a horizontal orientation, and the remaining acid yellow 17 solution was attached to the inflow tube of the fracture cast. The inflow and outflow tubes were re-opened to allow the acid yellow 17 solution to pass through the fracture cast at the pre-set pumping rate and the re-circulation system pump was turned down to a moderate mixing rate (Figure 3-11). A 1.5 mL sample was taken immediately using a disposable syringe (BD Syringe, ref# 309571) from the inlet sampling cell to record the influent acid yellow 17 concentration.

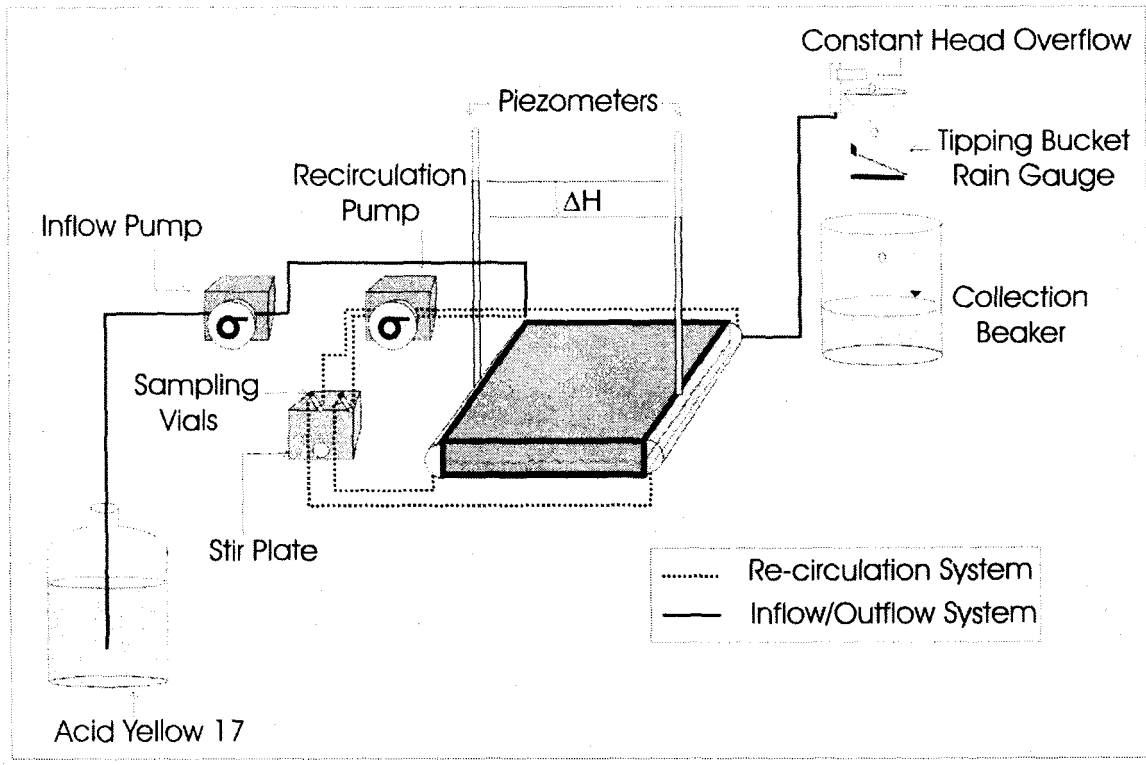

Figure 3-11: Schematic of acid yellow 17 tracer test.

Samples of 1.5 mL were withdrawn frequently (every 5-10 minutes) from the outlet sample vial using a disposable syringe for the first two hours of the test, after

which point most of tracer had passed through the system, and samples were required only every 20-30 minutes. The solution was withdrawn from the vial slowly so as not to induce false gradients into the system. The syringe was emptied into a disposable cuvette for absorbance determination using a spectrophotometer (Pharmacia LKB Biochrom Ltd.: 4054 Ultraspec Plus) at 400 nm (using the scan option for wavelength peak detection). Standard solutions were prepared (method 4110B, Standard Methods, 1998), and the instrument was calibrated periodically. The concentration of acid yellow 17 was obtained using a standard curve for acid yellow 17 concentrations against absorbance (Appendix A). Periodic samples were withdrawn from the influent sample cell throughout each experiment to ensure that the influent tracer concentration remained constant.

Each tracer test was performed with continuous flow and a constant influent acid yellow 17 concentration of 34 mg/L. Throughout the duration of each experiment, both the influent and effluent re-circulation systems were continuously running at moderate rates and the sample vials were mixed using a magnetic stir bar and plate. This process ensured complete mixing of the end-cap solution, therefore samples withdrawn from the influent and effluent sample cells were representative of the solution present in the influent and effluent end-caps respectively.

The tracer tests were sustained until complete breakthrough was achieved; that is, when the effluent concentration equalled the influent concentration. The effluent

concentration profile was used to determine the mass balance and the frictional loss apertures.

3.4 DNAPL ENTRAPMENT

Prior to applying the interfacial tracer technique, a known volume of DNAPL was trapped in the water-saturated fracture plane. The following section describes the materials, apparatus and method employed for the DNAPL entrapment phase of these experiments.

3.4.1. Materials

The DNAPL selected for the experiments was hydrofluoroether 7100 (HFE7100, 3M), because its physical and chemical properties are similar to those of many DNAPLs commonly found in the subsurface, yet it is non-toxic and therefore would not compromise the integrity of the epoxy transparent casts (Table 3-3). HFE7100 is a chemical containing a mixture of two ingredients: methyl nonafluoroisobutyl ether (CAS No 163702-08-7; 20-80%wt) and methyl nonafluorobutyl ether (CAS No. 163702-07-6; 20-80%wt).

Table 3-3: Physical and Chemical properties of HFE7100 (manufactured by 3M)

PHYSICAL PROPERTY	VALUE
Specific Physical Form	liquid
Odour, Colour, Grade	clear, colourless; slight ethereal odour
Density (g/mL)	1.5
Vapour pressure (mmHg) at 25°C	202
Solubility in water (ppm)	<12
Percent volatile (%)	100
Viscosity (cP) at 23°C	0.6
Boiling point (°C)	61
Melting point (°C)	-135
Flash point	None
Flammable limits	None

The deionized water used in the experiments was not buffered or autoclaved, as these experiments were relatively short term and therefore bacteria growth was not a concern. However, to minimize the potential for bacteria growth, the apparatus was covered in opaque plastic bags to prevent the presence of light.

3.4.2. Apparatus

The apparatus employed for the DNAPL entrapment was the same as that used for the hydraulic tracer tests, with the addition of a DNAPL release system and a DNAPL collection system (Figure 3-12).

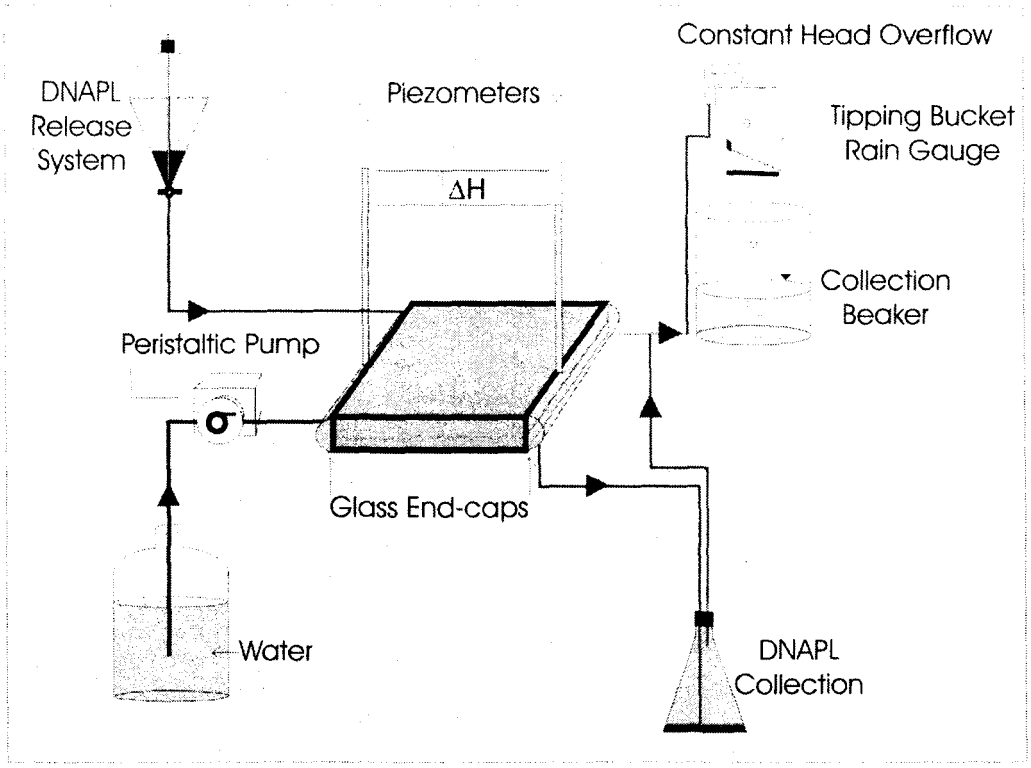

Figure 3-12: A schematic diagram of the experimental apparatus. Note that the dark grey colour represents the DNAPL.

The DNAPL release system was necessary for emplacing the DNAPL into the fracture plane at a constant head. This system consisted of a separatory funnel with a rubber stopper containing a steel tube that extended to the base of the separatory funnel. This system functioned as a Mariott bottle, maintaining a constant atmospheric pressure at the base of the separatory funnel. To ensure a constant head between experiments, the base of the steel tube was set to the same elevation as the effluent dropper on the downstream end of the experimental apparatus.

The purpose of the DNAPL collection system was to provide a means for collecting the DNAPL that passed through the fracture plane under a given hydraulic

head so that the mass of DNAPL trapped in the fracture could be accurately quantified using a mass balance approach. The DNAPL collection system consisted of an Erlenmeyer flask with a rubber stopper containing two stainless steel tubes, a short one extending to the bottom of the stopper, and a longer one extending just above the base of the flask. Tygon tubing was attached to the exposed ends of the steel tubes; the long steel tube was connected to the lower spigot of the effluent end-cap, and the short stell tube was connected to the effluent dropper. By placing the collection system at a lower elevation than the end-cap, the DNAPL that passed through the fracture plane could move under gravitational forces into the Erlenmeyer flask via the long steel tube, displacing the water in the Erlenmeyer flask to the system's outlet.

3.4.3. Methodology

A known volume of DNAPL was entrapped by performing the following three steps: water saturation, DNAPL release, and water flush. The fracture plane was saturated according to the procedure described in section 3.2.1. A known volume (200 mL and 250 mL in fractures 1 and 2 respectively) of the DNAPL (HFE7100) was set aside in preparation for the DNAPL emplacement procedure. During this time, the re-circulation system was inactive. In order to release the HFE7100 into the fracture, the separatory funnel was filled three quarters full with water and the tubing at the base of the separatory funnel was also filled with water. The separatory funnel base was closed with the stopcock. A funnel with a long stem was used to pour the HFE7100 below the water level in the separatory funnel so that no HFE7100 was lost to volatilization. The tubing at the

base of the separatory funnel was connected to the upper spigot of the influent end-cap. Prior to emplacement, the stopper containing the steel pipe was placed into the separatory funnel to ensure a constant head throughout the system for the emplacement process. At the same time the water flowing into the fracture system was disconnected and the separatory funnel was opened to allow the HFE7100 to flow into the influent end-cap.

As the HFE7100 moved into the influent end-cap, water was displaced towards the downstream end of the fracture. Any HFE7100 that exited the fracture plane migrated into the DNAPL collection system under gravitational forces. Once all the HFE7100 in the separatory funnel had entered the fracture, the stopcock on the separatory funnel was closed, the stopper was removed, and more water was added in preparation for the water flush.

The purpose of the water flush was to employ high hydraulic gradients in an attempt to mobilize as much of the HFE7100 trapped in the fracture as possible. To mobilize the HFE7100, the height of the separatory funnel was raised which increased the hydraulic gradient across the fracture plane, thereby mobilizing some of the trapped HFE7100 mass. The head loss and time elapsed were recorded for the duration of the water flush.

To calculate the mass of HFE7100 trapped in the fracture plane, it was necessary to collect the HFE7100 that passed through the fracture. In order to do so, the inflow and

outflow tubes were closed using clamps. The HFE7100 collected in the DNAPL collection system was poured into a separatory funnel along with the HFE7100 that collected in the lower spigot of the influent end-cap. A mass balance was conducted to determine the mass of HFE7100 that remained trapped in the fracture after the water flush. The entrapped HFE7100 was expressed as a percent of the fracture volume using the following equation:

$$\%HFE = \left(1 - \frac{V_F - \left(\frac{M_H}{\rho_H} \right)}{V_F} \right) x100\% \qquad (3\text{-}2)$$

where V_F [L^3] is the fracture volume, M_H [M] is the mass of HFE7100 entrapped, and ρ_H [$M \cdot L^{-3}$] is the density of HFE7100.

3.5 INTERFACIAL TRACER TESTS

The purpose of the interfacial tracer test was to measure the area at the interface between the entrapped HFE7100 and water. The results from these experiments were compared against and calibrated with the direct interfacial area measurement obtained from the image analysis using software. This section presents the materials and methodology employed for the interfacial tracer tests.

3.5.1. Materials

The interfacial tracer used in this experiment was sodium dodecylbenzene sulphonate, SDBS (BDH Chemicals Ltd, >99% pure), and the non-reactive tracer was acid yellow 17 as the non-reactive tracer. SDBS was chosen because it has been successful as an interfacial tracer in several porous media studies (Annable et al., 1998a; Annable et al., 1998b; Saripalli et al., 1997b; Kim et al., 1999). SDBS is a long carbon chain and a benzene ring with a sulphate group, representing the hydrophobic tail and hydrophilic head of the compound respectively (Figure 3-13). SDBS readily adsorbs at fluid-fluid interfaces forming monolayers with the hydrophilic head groups oriented toward the aqueous phase.

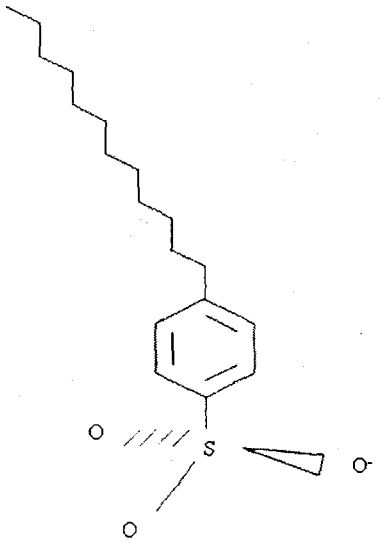

Figure 3-13: The chemical structure of the sodium salt of dodecylbenzenesulfonate (SDBS) used in the interfacial tracer tests.

The influent concentration of SDBS used in these experiments was 45 mg/L, which is well below the critical micelle concentration of 418 mg/L. This low concentration ensured that SDBS would readily adsorb in monomeric form at the fluid-fluid interfaces. Acid yellow 17 (cas#:6359-98-4, Sigma-Aldrich Canada Ltd.) was selected as the non-reactive tracer since it proved to be non-reactive in the fracture cast in a number of preliminary tests.

For each experiment, the fracture cast and experimental set-up was placed on top of a light table so that a photo of the entrapped HFE7100 could be taken at the end of the interfacial tracer test for verification of the interfacial area, a_{nw} obtained experimentally. Between experiments, the fracture cast was flushed with 20 L of 0.1% v/v bleach to remove any residual tracer solution and to eliminate bacteria growth. The fracture cast was also flushed with deionized water overnight prior to commencing each experiment.

3.5.2. Interfacial Tracer Experiments

Once the HFE7100 was entrapped, the interfacial tracer technique was applied to determine the contact area between the HFE7100 and water in the fracture plane. The interfacial tracer technique employed the same steps as the tracer test for aperture determination (Section 3.3.2.) except this time DNAPL was present. The four steps include: steady state aqueous flow, tracer release, stepwise tracer input and sampling over time.

After the HFE7100 was entrapped, the DNAPL release and DNAPL collection system were removed. Water flow was re-established at approximately 0.6 mL/min. Once it had reached steady state, the two tracer tests were performed sequentially: the reactive interfacial tracer test was conducted first using SDBS, followed by the non-reactive interfacial tracer test using acid yellow 17. The interfacial tracer tests were conducted separately for accurate quantification of SDBS. This two-step approach to tracer tests is a common practice in the porous media literature (Saripalli et al., 1998; Saripalli et al., 1997b; Kim et al., 1999).

The procedure for the SDBS interfacial tracer test was the same as the tracer test for aperture determination described in Section 3.3.2., however in this case input SDBS concentrations of 27 mg/L to 42 mg/L was employed at 0.6 mL/min and 2.5 mL/min in fractures 1 and 2 respectively. Samples of 1 mL were collected from the effluent sample cell approximately every 5-10 minutes for the first 3 hours, and then every 20-30 minutes for the next 6-11 hours until breakthrough was achieved. The samples were placed in 1.5 mL vials with screw cap lids containing septums (part no. C223700C (vials), C223710C (lids), C242C (septa), Chromatographic Specialies Inc.). At this point, deionized water was reconnected at the inflow and allowed to pass through the system. Sampling was continued until the effluent SDBS concentration equalled the influent SDBS concentration.

The samples containing SDBS were analyzed using a HPLC (high performance liquid chromatograph) followed by fluorescence detection. The HPLC separation conditions were installed to analyze linear alkylbenzene sulphonates, such as SDBS (Table 3-3), where the lower limit of detection is 5 ng/dm^3 (Hummel, 2000).

Table 3-3: HPLC separation conditions for SDBS (Hummel, 2000).

Components of HPLC	Specifications
Column	Type: RP-18; 250mm long; 4.6mm ID; 0.005mm particle size
Eluent	Methanol/water 21:4 (v/v); 0.0857M
Flow	1cm^3/min
Detector	Fluorescence ex = 232nm, em = 290nm

The area under the peaks for each homolog of SDBS was summed as this total area is correlated to the concentration of SDBS present. Standard solutions of SDBS ranging from 0-100 mg/L were prepared (method 4110B, Standard Methods, 1998), and the HPLC was calibrated periodically. The concentration of SDBS in the interfacial tracer test samples was obtained using the standard curve for SDBS concentration (Appendix A).

After completion of the SDBS interfacial tracer test, water was allowed to flow through the fracture cast overnight, and the acid yellow 17 interfacial tracer test was performed the following day. The acid yellow 17 interfacial tracer test was conducted in the same manner as described in Section 3.3.2., using 34 mg/L of acid yellow 17 at 0.6

mL/min and 2.5 mL/min in fractures 1 and 2 respectively. Once the SDBS and acid yellow 17 breakthrough curves were obtained, the chromatographic separation between these curves was used to calculate the interfacial area, a_{nw} between the entrapped HFE7100 and surrounding water.

3.5.3. Interfacial Tension (γ) Measurement

The Drop Volume Method (Drop Volume Tensiometer TVT1, Lauda) was used to measure the interfacial tension between HFE7100 and SDBS. Aqueous solutions of SDBS were prepared in deionized water in the 0-120 mg/L concentration range. The drop volumes were recorded after 30 s of drop time.

3.5.4. Interfacial Area –Photo Analysis

In order to verify the experimental a_{nw} value, a digital photo of the trapped HFE7100 was required. However, because the HFE7100 could not be dyed due to its unique chemical properties, 10 mg/L red-dyed water (15-11890-4, Dawn) was pumped into the fracture cast for visual observation of the entrapped HFE7100 (Figure 3-14). The red-dyed water was pumped at the same rate used in the IFTT so as not to disturb the entrapped DNAPL mass. After a few hours, the red-dyed water was uniform throughout the fracture cast (Figure 3-14).

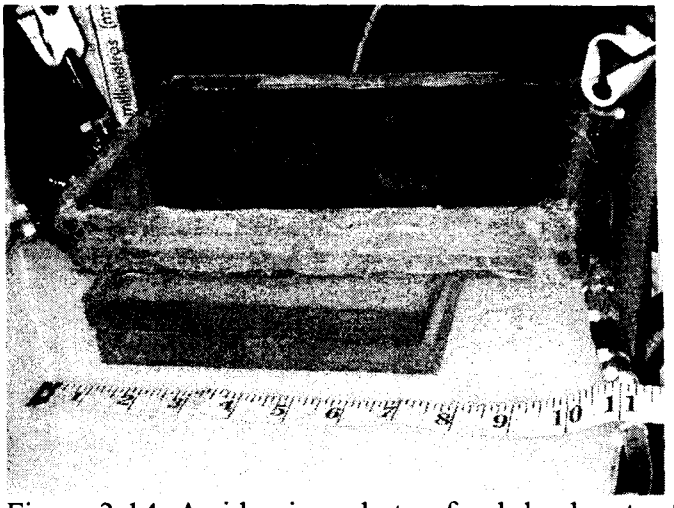

Figure 3-14: A side-view photo of red-dyed water flowing through the fracture cast with HFE7100 entrapped (seen as the colourless phase).

At this point the light table was turned on and a high resolution digital photo with a real scale was taken. The digital image was imported into the ImageTool software (Image Tool by UTHSCSA, version 3.00), where it was manipulated using the software options to obtain the sharpest interface. By calibrating the software using the scale in the photo and tracing the circumference of each HFE7100 blob, the total distance of the HFE7100 in contact with water was determined. The interfacial area was calculated based on the assumption that each blob formed a disc with a thickness equal to the equivalent mass balance aperture:

$$A = e_{mb} P + \frac{P^2}{2\pi} \tag{3-1}$$

where A [L^2] is the total blob surface area, P [L] is the blob perimeter and e_{mb} [L] is the mass balance aperture.

Because the a_{nw} value is commonly expressed as the interfacial area per volume of the system in the literature (Saripalli et al., 1998; Saripalli et al., 1997b; Kim et al., 1999), the calculated interfacial area, A [L^2] was divided by the fracture volume, F_r [L^3] and reported as the fluid-fluid interfacial area, a_{nw} value [$L^2 \cdot L^{-3}$]:

$$a_{nw} = \frac{A}{F_r} \tag{3-2}$$

This value was compared to a_{nw} values obtained experimentally as a verification of the interfacial tracer technique for fractured rock systems.

CHAPTER 4: RESULTS AND DISCUSSION

This chapter presents the results of this research, including the fracture plane characterization, the interfacial tracer tests and the digital photo analysis and discusses the significance of these results. The goal of the hydraulic and tracer tests was to characterize the fracture aperture field. These tests provided three distinct aperture values as defined by Tsang (1992): the equivalent hydraulic aperture, the mass balance aperture, and the frictional loss aperture. The interfacial tracer technique was developed as a tool to estimate the fluid-fluid interfacial area, a_{nw} in fractured rock environments. Finally, an a_{nw} obtained through digital photo analysis was compared to the results of the interfacial tracer technique for verification purposes.

4.1 FRACTURE PLANE CHARACTERIZATION

As discussed in Chapter 3, two transparent casts were fabricated for this experimental work, one from a limestone fracture and one from a granite fracture. The limestone and granite casts will be referred to as fracture 1 and fracture 2 respectively throughout this chapter. The dimensions and end cap volumes of each of these fractures are presented in Table 4-1. Both fracture casts were characterized using hydraulic studies to determine the equivalent hydraulic aperture, and tracer studies to determine the mass balance and frictional loss apertures. The results of these tracer studies are described in the following sections.

4.1.1 Hydraulic Studies

The hydraulic studies are based on the well-known bulk cubic law for fluid flow through parallel plates. The cubic law is a simple linear flow law which predicts that the flow rate is proportional to the cube of the aperture, assuming that the fracture plane is well represented by parallel plates. The hydraulic aperture that satisfies the bulk cubic law is given by (Snow, 1965):

$$e_h = \left(\frac{12\mu QL}{\rho g W |\Delta H|} \right)^{\frac{1}{3}} \tag{4-1}$$

where μ [$M \cdot L^{-1} \cdot T^{-1}$] is the dynamic viscosity, Q [$L^3 \cdot T^{-1}$] is the flow rate, L [L] is the fracture length, W [L] is the fracture width, ρ [$M \cdot L^{-3}$] is the fluid density, g [$L \cdot T^{-2}$] is the acceleration due to gravity, and ΔH [L] is the head loss across the length of the fracture plane. Equation (4-1) assumes that the cubic law is valid, whereby the fracture is well represented by parallel plate walls, the fracture is horizontal, and the matrix flow is negligible.

Because the Cubic Law was developed assuming a 1-D fracture rock system with parallel plate fracture walls, inertial forces acting on the bulk fluid are ignored. In natural fractures, the fracture surface typically has various undulations causing surface roughness, which thereby contribute to inertial forces. For this reason, a number of researchers have attempted to validate the cubic law for describing flow through natural fractured rock systems (e.g., Brush and Thomson, 2003; Konzuk and Kueper, 2004; Zimmerman and Yeo, 2000). In general the aforementioned studies indicate that the bulk

cubic law is valid when applied at the single-fracture scale for laminar flow conditions. However, surface roughness can influence the inertial forces on the bulk flow, which implies that caution must be taken when applying the cubic law to variable aperture fractures (Brush and Thompson, 2003). As a result, the hydraulic aperture derived from these experiments is considered an estimate of the effective aperture field only.

The hydraulic studies indicate a linear relationship between the specific discharge and head loss across the fracture plane for a large range of flow rates in both fractures 1 and 2 (Figures 4-1a and 4-1b respectively). The specific discharge remained linear with respect to head loss for 0-70 cm/min in fracture 1 and 0-20 cm/min in fracture 2. This linear relationship indicates that the influence of the inertial forces on the bulk flow rate is small in these ranges for fractures 1 and 2 respectively, and therefore the Cubic Law should provide a reasonable estimate of the equivalent hydraulic aperture within these specific discharge ranges. However, at values above 70 cm/min in fracture 1 and above 20 cm/min in fracture 2 (Figure 4-1a and 4-1b respectively), the specific discharge was no longer linear in relation to head loss, indicating that inertial forces become important at these higher discharge rates and the bulk cubic law is no longer valid.

The Reynolds Number, Re is a ratio of inertial to viscous forces, and is an indicator of flow regime. In fractured environments, the Re is calculated as follows (de Marsily, 1986):

$$\mathrm{Re} = \frac{2e_h u}{\nu} \qquad (4\text{-}2)$$

where e_h [L] is the aperture width, u [$L \cdot T^{-1}$] is the average linear velocity represented by the specific discharge, v is the kinematic viscosity [$L^2 \cdot T^{-1}$]. Figures 4-1a and 4-1b illustrate the Re numbers corresponding to the range of specific discharge. Typically, in porous media systems Re numbers less than 10 indicate laminar flow. However this relationship is not directly applicable to fracture rock systems, therefore the Re numbers plotted in Figure 4-1a and Figure 4-1b act only as a guide for laminar flow conditions.

In fracture rock systems a linear plot of specific discharge against head loss is indicative of laminar flow. For all discharge values below 70 cm/min in fracture 1 and below 20 cm/min in fracture 2, a linear relationship between specific discharge and head loss is apparent, and therefore laminar flow conditions. However as evidenced by the curve in Figure 4-1b, the ΔH becomes non-linear after approximately 20 cm/min, which indicates that the flow is no longer laminar.

Table 4-1a: Three apertures calculated for the same valid specific discharge, q range. Note that W (perpendicular to flow) and L (parallel to flow) refer to the fracture width and length respectively.

Fracture	Original Fracture Material	W (cm)	L (cm)	Valid q (cm/min) Range	e_f (μm)		e_{mb} (μm)		e_h (μm)		δ (-)
					Calc.	St. Dev.	Calc.	St. Dev.	Calc	St. Dev.	
1	Limestone	14.7	24.5	0-70	149	+/- 29	12,934	+/- 12,732	515	+/-136	0.004
2	Granite	22.4	34.5	0-20	171	+/- 22	16,483	+/- 14,659	699	+/-193	0.01

Although the three aperture values reported in Table 4-1a for the valid range of specific discharge, a significant error was introduced in the calculations of e_{mb} and e_f as they rely on the t_m value from the tracer tests. Because the t_m value was obtained for flow rates of 0.6 mL/min and 2.5 mL/min for fracture 1 and 2 respectively, it is inconceivable that the same t_m values apply to higher flow rates. As a result, the aperture values reported in Table 4-1 provide an estimate of the apertures only. The actual aperture values calculated for the valid q range and the valid t_m values are reported in Table 4-1b.

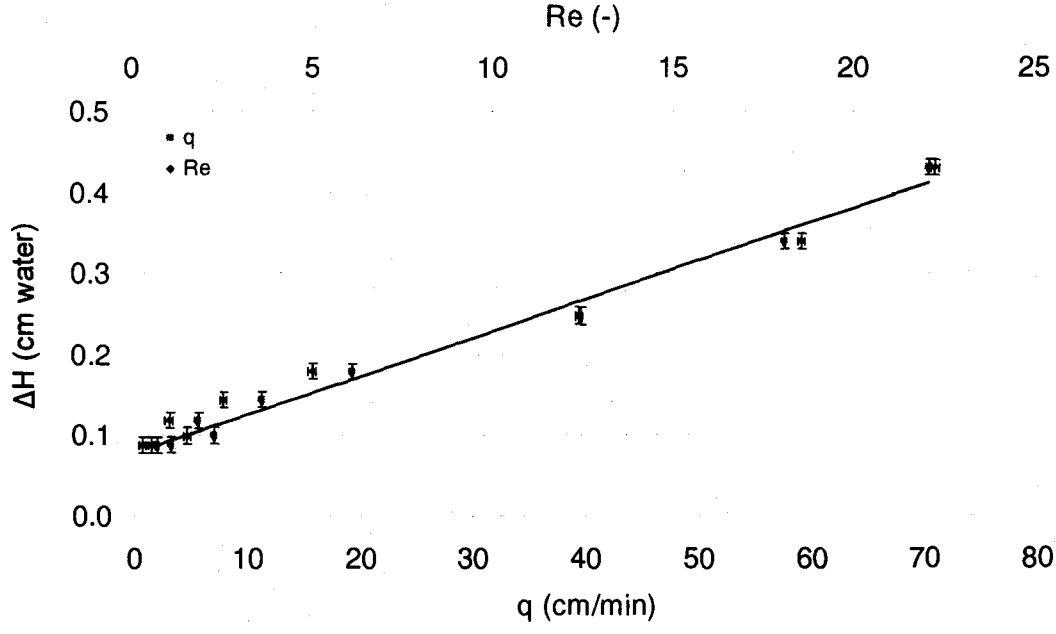

Figure 4-1a: Head loss across fracture 1 in response to specific discharge (q) and Reynolds Number (Re). The q calculation was based on e_h, where $q = Q/We_h$. The linear relationship had an R^2 of 0.988. The Re was calculated using (4-2). The error bars were estimated based on the measurement error in head loss and flow readings.

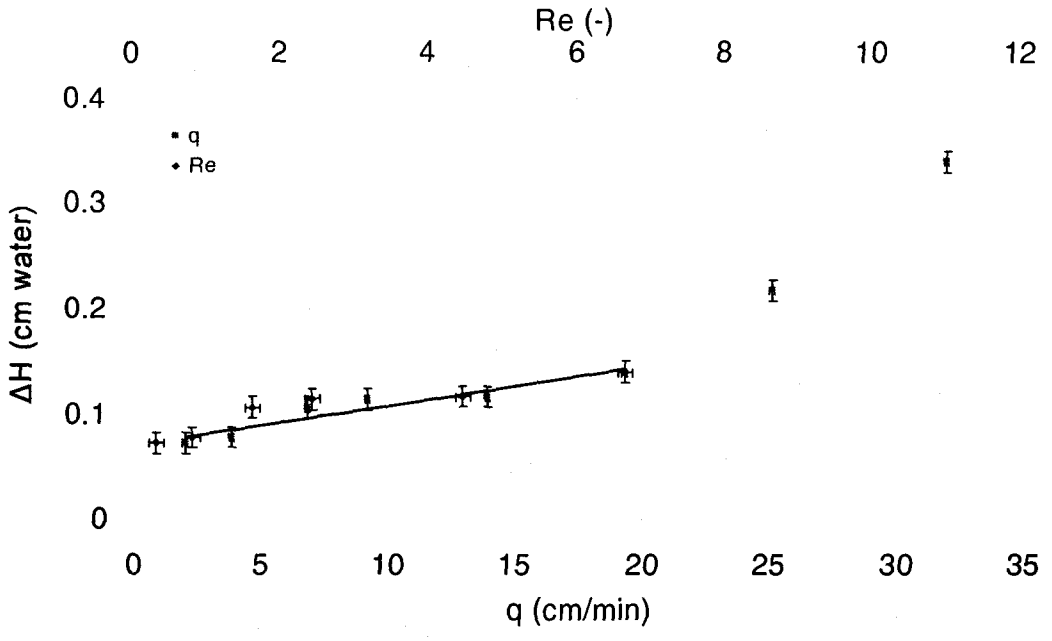

Figure 4-1b: Head loss across fracture 2 in response to specific discharge (q) and Reynolds Number (Re). The q calculation was based on e_h, where $q = Q/We_h$. The linear relationship had an R^2 of 0.9006. The Re was calculated using (4-2). The error bars were estimated based on the measurement error in head loss and flow readings.

Table 4-1b: Actual apertures calculated for the valid q range and the valid t_m values.

Fracture	Original Fracture Material	q (cm/min)	e_f (μm)	e_{mb} (μm)	e_h (μm)	δ (-)
1	Limestone	0.78	499	858	598	0.58
2	Granite	2.43	189	2,347	438	0.08

4.1.2. Tracer Studies

Recall that the effluent sample was withdrawn from the flow-through sampling vial located within the recirculation system loop. The measured tracer concentration at the sampling vial is not representative of the concentration exiting the fracture plane.

Instead, it represents a concentration diluted by the combined volume of the end-cap and re-circulation system. For this reason, the tracer concentration measured in the sampling vial was manipulated to back-calculate the tracer concentration leaving the fracture plane. This was accomplished using a mass balance approach for a flow-through mixing cell (Dickson, 2001):

$$C_f(t) = \frac{V}{Q}\frac{dC_c(t)}{dt} + C_c(t) \cong \frac{V}{Q}\left(\frac{C_c^{t+\Delta t} - C_c^{t-\Delta t}}{2\Delta t}\right) + C_c^t \qquad (4\text{-}3)$$

where $C_f(t)$ [M·L^{-3}] is the tracer concentration exiting the fracture plane, $C_c(t)$ [M·L^{-3}] is the concentration measured from the sampling cell of the effluent end-cap and re-circulation system, V [L^3] is the combined volume of the effluent end-cap, re-circulation system, and sampling cell, Δt [T] is the time between sampling events, and Q [L^3·T^{-1}] is the flow rate through the system. All effluent concentrations reported in this thesis have been adjusted to represent the tracer concentration exiting the fracture plane; in doing so, a degree of error was introduced since the estimated C_f values are sensitive to small variations in the temporal slope in (4-3). Appendix C includes raw and adjusted tracer data.

The tracer data were required for calculating two equivalent aperture values: the mass balance aperture, e_{mb}, and the frictional loss aperture, e_f. The mass balance aperture assumes that the aerial extent of the fracture plane in which the tracer travels is known. Thus the mass balance aperture relies only on the mass balance physical law and is related to pore volume of the fracture. It is defined as (Tsang, 1992):

$$e_{mh} = \frac{Qt_m}{LW} \tag{4-4}$$

where t_m [T] represents the mean tracer residence time, and was calculated using moment analysis.

The frictional loss aperture involves expressing the mean tracer residence time, t_m in terms of the transport velocity, and assumes that the flow through rough-walled fractures is well represented by the cubic law. The frictional loss aperture, e_f is calculated from the head loss measurement, the tracer path length, the mean tracer residence time, and the fluid density and viscosity (Tsang, 1992):

$$e_f = L\sqrt{\frac{12\mu}{\rho g|\Delta H|t_m}} \tag{4-5}$$

The breakthrough curves for acid yellow 17 in fractures 1 and 2 are provided in Figure 4-2a and Figure 4-2b respectively. The effluent tracer concentrations in Figure 4-2a and Figure 4-2b were normalized using the average influent tracer concentration listed in Table 4-2, after which they were adjusted using (4-3). The tracer breakthrough curves display significantly more variability than the raw breakthrough curves provided in Appendix C. This variability can be attributed to the fact that the derivative in (4-3) magnifies small variations in the temporal slope of the raw data. The influent concentrations, normalized using the average influent concentration, tend to take some time to reach unity, indicating that the recirculation system is not mixing the influent

solution efficiently. This may be due to blockages in the re-circulation system, or to the method employed to achieve a uniform initial tracer concentration.

The frictional loss and mass balance apertures were derived from the acid yellow 17 tracer tests. Table 4-1b provides the experimental conditions for each tracer test, and the frictional loss and mass balance aperture that ensued. The flow rates selected for the tracer tests were chosen to match the flow rates employed in the interfacial tracer tests to ensure that the same hydrodynamic conditions were present. For comparison purposes, the hydraulic apertures corresponding to these hydrodynamic conditions are also provided in Table 4-1b.

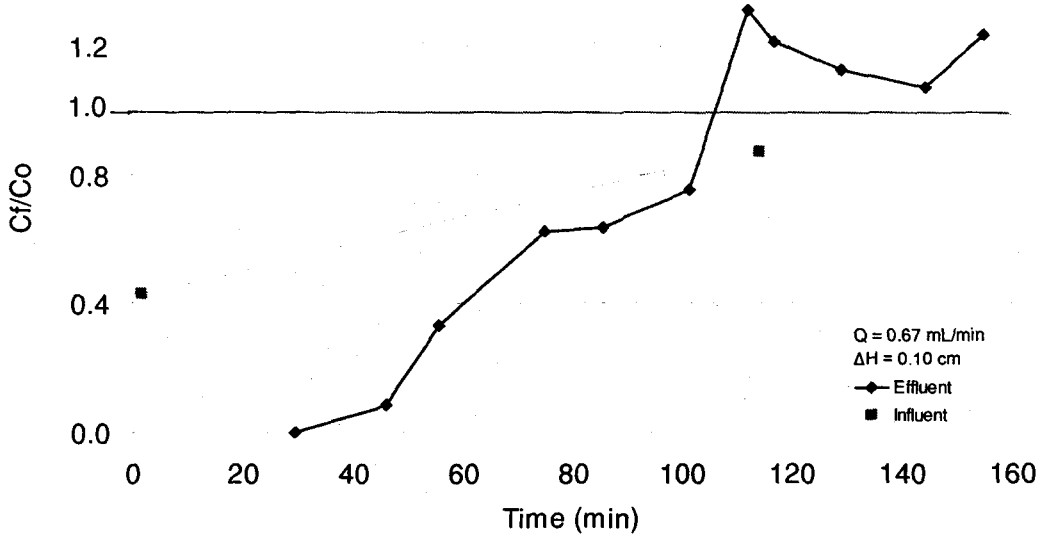

Figure 4-2a: Breakthrough curve for acid yellow 17 in fracture 1. Note the influent concentration took some time to reach unity, therefore for the average influent concentration for 0-114 minutes was used to normalize the effluent concentrations in this time period, and the overall average influent concentration was used to normalize the remaining effluent concentrations. These influent averages were selected to best represent the average influent concentration for these specific time periods.

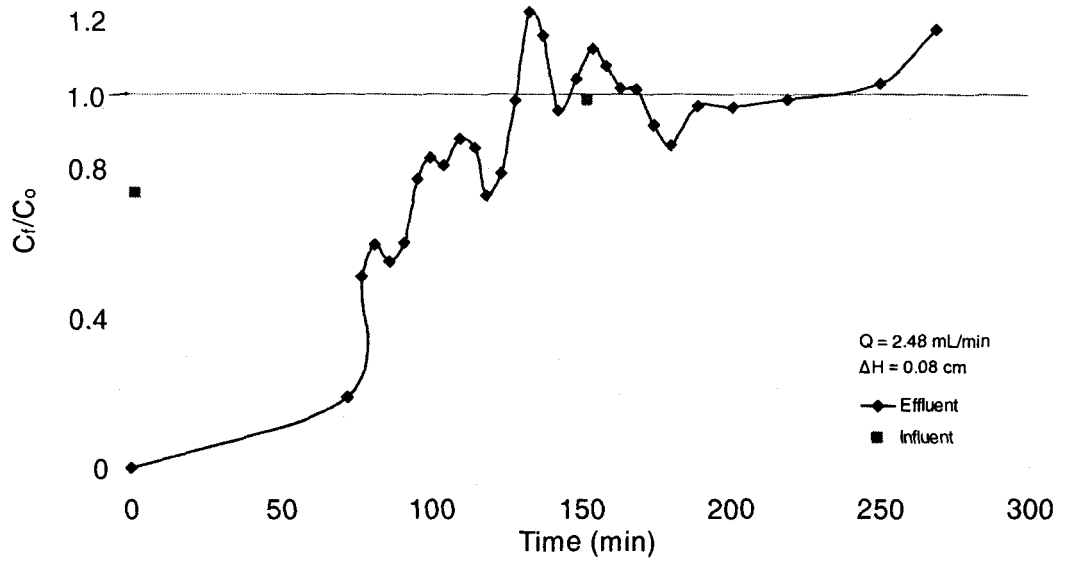

Figure 4-2b: Breakthrough curve for acid yellow 17 in fracture 2. Note that no average influent concentration adjustments were necessary here since the influent concentration reach unity relatively quickly.

A comparison of the three equivalent apertures: frictional loss, mass balance and hydraulic, for both fractures 1 and 2, reveals the following relationship:

$$e_{mb} > e_h > e_f$$

This relation between the three equivalent apertures has been reported by others (Tsang 1992; Dickson, 2003; Brush, 2000). The different magnitudes, obtained for the three equivalent apertures are a result of the different approaches used to derive each aperture value (Tsang, 1992). One obvious difference is that the hydraulic and frictional loss apertures are based on the head loss across the fracture plane, while the mass balance aperture is not. For this reason, the hydraulic and frictional loss apertures are sensitive to the regions of high head loss, which occurs in small aperture regions. Therefore the

hydraulic and frictional apertures are sensitive to local heterogeneities and are weighted towards the smaller apertures along the flow path. In contrast, the mass balance aperture is dependent on the mass of tracer stored in the void space, which characteristically occurs in large aperture regions. As a result, the mass balance aperture represents an average aperture along the general flow path of the tracer. All three apertures are commonly labelled 'equivalent aperture' in the literature, although there is discrepancy as to which one best describes the aperture field. According to Tsang (1992) the mass balance aperture provides the best estimate of the arithmetic mean aperture, and is therefore most worthy of being called an equivalent aperture.

By comparing the frictional loss and mass balance apertures in ratio form, an expression of extreme aperture regions is achieved. The ratio of the frictional loss aperture to the mass balance aperture is termed the tracer aperture ratio, δ; it provides a ratio of the smallest aperture regions to largest aperture regions along the tracer flow pathway, and is given by (Dickson and Thomson, 2003):

$$\delta = \frac{e_f}{e_{mb}} \tag{4-6}$$

This ratio is descriptive, since it is the extreme aperture regions that are responsible for controlling flow pathways and solute transport. Smaller tracer aperture ratios indicate more variability along the tracer flow path, whereas larger tracer aperture ratios indicate less variability along the tracer flow path. A parallel plate fracture, which has no extreme aperture regions, would have a tracer aperture ratio of one. The tracer aperture ratios for

fractures 1 and 2 reveal that fracture 2 has a larger range of extreme aperture regions than fracture 1 (Table 4-1b).

4.1.3. Fracture Volume Determination

The acid yellow 17 tracer tests were also used to estimate the volume of the fracture casts. Because the mass balance aperture relies on the volume of pore space, it can be manipulated to estimate the fracture volume by rearranging (4-4) and solving for volume:

$$V_{fracture} = e_{mb} LW = Qt_m \tag{4-7}$$

where e_{mb} is the mass balance aperture corresponding to the flow rate employed in the acid yellow 17 tracer test. The fracture volumes for fracture 1 and 2, calculated using (4-7) are reported in Table 4-2.

Table 4-2: Fracture volumes based on the mass balance aperture calculation.

Fracture	L (cm)	W (cm)	Q (mL/min)	C_o (mg/L)	t_m (min)	e_{mb} (cm)	$V_{fracture}$ (mL)
Fracture 1	24.5	14.7	0.689	16.7 * ; 25.7†	65.0	0.0858	44.8
Fracture 2	34.5	22.4	2.48	31.1	76.0	0.235	181

*for first 0-114 minutes of tracer test, †for remainder of tracer test

4.2. DNAPL ENTRAPMENT

Prior to conducting the interfacial tracer tests, it was necessary to establish a mass of trapped DNAPL in the fracture casts. In order to entrap the DNAPL, HFE7100 a

known volume of HFE7100 was released into the fracture plane under a capillary pressure of approximately 2.4 cm of water in fracture 1 and 0.5 cm of water in fracture 2. Once all of the HFE7100 was released into the system, water was flushed through the fracture in an attempt to mobilize as much HFE7100 as possible.

Three HFE7100 entrapment procedures were performed: two were conducted on fracture 1 and another was carried out on fracture 2. Experiment 1 and 3 were performed while the fracture was in horizontal position, and experiment 2 was conducted with fracture 1 inclined at a 20° angle. The purpose of inclining the fracture was to initiate a different entrapped HFE7100 morphology through introducing gravitational forces. Experiment 2 was important since inclined fractures are ubiquitous in natural fractured rock environments. Table 4-3 provides the experimental conditions and resulting mass of trapped HFE7100 from the three DNAPL entrapment procedures.

Table 4-3: Summary of the experimental conditions and results for the HFE7100 entrapment experiments.

Exp No.	Fracture Name	N_c (-)	Release P_c (cm H_2O)	HFE7100 Entrapped (mL)	Fracture Volume (mL)	% of Fracture with HFE7100
1	Fracture 1	1.06×10^{-5}	2.4	27.6	45	62
2	Fracture 1	N/A	2.5	23.1	45	52
3	Fracture 2	1.46×10^{-5}	0.5	29.7	181	20

The force responsible for trapping HFE7100 masses in these experiments is the capillary pressure. The viscous forces imposed by the flowing aqueous phase act to mobilize the entrapped HFE7100. In the case of horizontal flow, where gravitational forces are negligible, the flushing capillary number, N_c is an appropriate measure of the HFE7100's ability to migrate as it represents the ratio of viscous to capillary forces acting on the HFE7100 mass. The N_c was reported for experiments 1 and 3 only as they were performed under horizontal flow conditions. At the start of each of these experiments, N_c was low, then it gradually increased as the hydraulic head across the fracture plane was increased. Throughout this time, mobilized HFE7100 exited the fracture plane. However, once the maximum flushing N_c was reached as reported in Table 4-3, the HFE7100 remaining in the fracture plane could not be mobilized. The maximum N_c was on the order of $1x10^{-5}$ for experiments 1 and 3, which is small in comparison to studies by Longino (1998) and Longino and Kueper (1999) who reported mobilization at capillary numbers as high as $1x10^{-3}$. However, the data are in agreement with Dickson (2001) who reported no further mobilization could be achieved when capillary numbers were increased beyond $1x10^{-3}$ to $1x10^{-5}$.

Throughout the DNAPL entrapment procedure, two dynamic processes were observed. Firstly, the HFE7100 pinched off due to decrease in capillary pressure upon entering a larger aperture region. Secondly, the HFE7100 that passed through the fracture plane, exited not as a continuous mass, but as single droplets at specific points along the fracture face. The exit points appeared to be consistent in repeat HFE7100 emplacement

experiments, suggesting that there is a heterogeneous distribution of flow paths inherent to each fracture plane. These observations agree with those reported by Dickson (2001).

The morphology of the entrapped HFE7100 mass remained relatively constant after the water flush, indicating that the HFE7100 mass was indeed trapped in the fracture plane. Table 4-3 reports the calculation as a fraction of the fracture volume using (3-2). The percent of fracture 1 containing HFE7100 was similar in experiments 1 and 2, even though the fracture was tilted in experiment 2. It is likely that the gravitational forces imposed by the small incline were not large enough to overcome the required capillary pressures. The percent of the fracture containing HFE7100 varied significantly between fracture 1 and 2, as expected, since the retention capacity varies with the aperture field characteristics of individual fracture planes.

Figures 4-3a through 4-3c illustrate the trapped HFE7100 morphologies from experiments 1 through 3 respectively. A number of factors, including the aperture field geometry, the fluid-fluid properties (interfacial tension, and viscosity density of the fluids), fluid-solid properties (wettability), and external forces on the fluids (pressure gradients and gravity) all play a role in controlling the size and shape of the entrapped HFE7100. In addition, high *Nc* values may contribute to the morphology of the entrapped HFE7100. According to Dickson (2001), the pressure gradient at high *Nc* values could push a large HFE7100 blob into a pore throat, causing smaller drops to break off and become trapped, while the remaining HFE7100 blob redistributes itself into smaller

blobs. This could be a contributing factor for HFE7100 configurations in all experiments as a number of small HFE7100 blobs were observed in each case.

Figure 4-3a: Plan view of the HFE7100 entrapped in fracture 1, experiment 1. The HFE7100 is represented by the colourless liquid, while the aqueous phase has been dyed red (as seen as the dark grey colour).

Figure 4-3b: Plan view of the HFE7100 entrapped in fracture 1 inclined at a 20° angle, experiment 2. The HFE7100 is represented by the colourless liquid, while the aqueous phase has been dyed red (as seen as the dark grey colour).

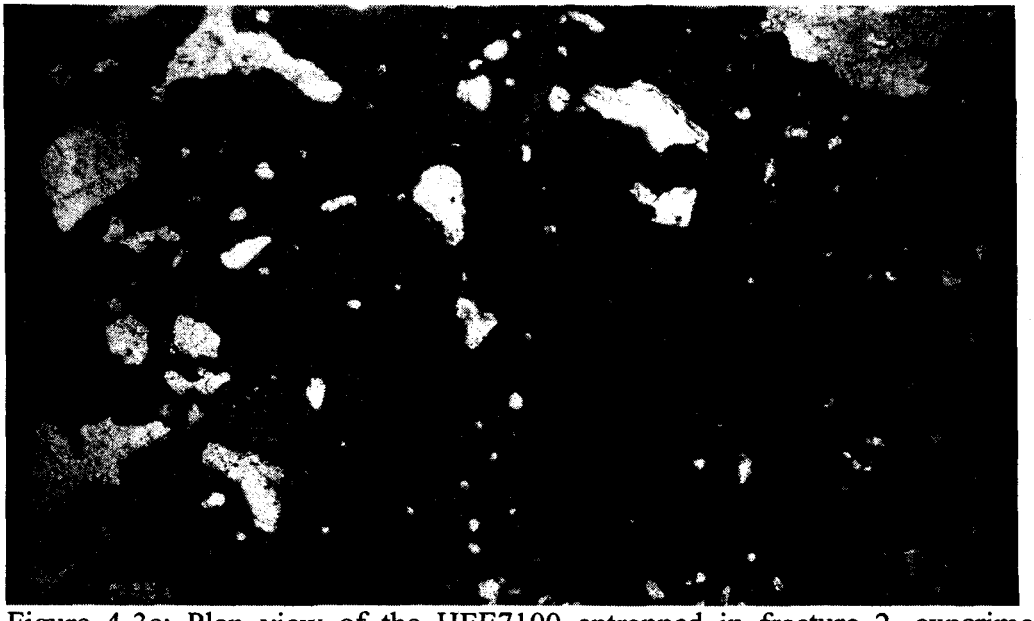

Figure 4-3c: Plan view of the HFE7100 entrapped in fracture 2, experiment 3. The HFE7100 is represented by the colourless liquid, while the aqueous phase has been dyed red (as seen as the dark grey colour). Note the large pinkish-white blob in the upper right corner of the picture is the upper boundary of the fracture plane, not a HFE7100 blob.

4.3. INTERFACIAL TRACER TESTS

The interfacial tracer tests consisted of three parts: SDBS solution-HFE7100 interfacial tension measurements, background SDBS adsorption tests, and the SDBS interfacial tracer tests. The SDBS solution-HFE7100 interfacial tension measurements were important for determining the interfacial tracer distribution coefficient, $K_{i,}$ required for the a_{nw} calculations. Background SDBS tracer tests, in the absence of HFE7100 were performed, to quantify the loss of SDBS due to adsorption to the experimental set-up. The following sections describe the results from the preliminary procedures, along with the results from the interfacial tracer tests themselves.

4.3.1. Interfacial Tracer Distribution Coefficient, K_i

Because the interfacial adsorption isotherm for SDBS is a strong non-linear function of the bulk concentration for most fluid-fluid interfaces, it is important to utilize an interfacial adsorption coefficient, K_i, which optimally represents the distribution characteristics of the tracer between the bulk phase at the fluid-fluid interface. The K_i value was necessary for the interfacial area, a_{nw} calculations; it was achieved through measurements of the interfacial tension, γ between HFE7100 and SDBS solutions ranging in concentration from 0 to 120 mg/L. The data are plotted in Figure 4-4a; it illustrates that the interfacial tension decreases exponentially with increasing SDBS concentration. Since the γ-C relationship is nonlinear, the adsorption isotherm is nonlinear (Kim et al, 1999; Kim et al., 1997; Saripalli et al., 1998). Therefore K_i must be estimated at each input concentration by taking the slope of the line ($d\gamma/dC$) at the initial tracer concentration, C_o;

this was achieved by fitting the measured γ vs. C data to an exponential model (Saripalli et al., 1998; Kim et al., 1997):

$$[\gamma = \alpha - \beta \ln(C)] \tag{4-7}$$

where $C = C_o < CMC$ [mol·L^{-3}] is the SDBS concentration and β represents the slope of the line ($d\gamma/dC$). The derivative of (4-7) was substituted into (2-13) to obtain an approximated K_i as follows (Kim et al, 1997; Saripalli et al., 1998):

$$K_i = \frac{\beta}{2RTC_o} \tag{4-8}$$

Data points from the fitted model were then employed in (4-8) to obtain an adsorption distribution coefficient K_i corresponding to a given C_o.

The measured data for decrease in HFE7100-SDBS interfacial tension with increase in SDBS concentration are provided in Figure 4-4a. The data fiteted to the exponential model are provided in Figure 4-4b. The slope of the regression fit is 7.32, which is in agreement with reported values for interfacial tension data for two similar DNAPL-SDBS solutions, as reported in Table 4-4. The K_i calculated for each experiment's input tracer concentration is reported in Table 4-5.

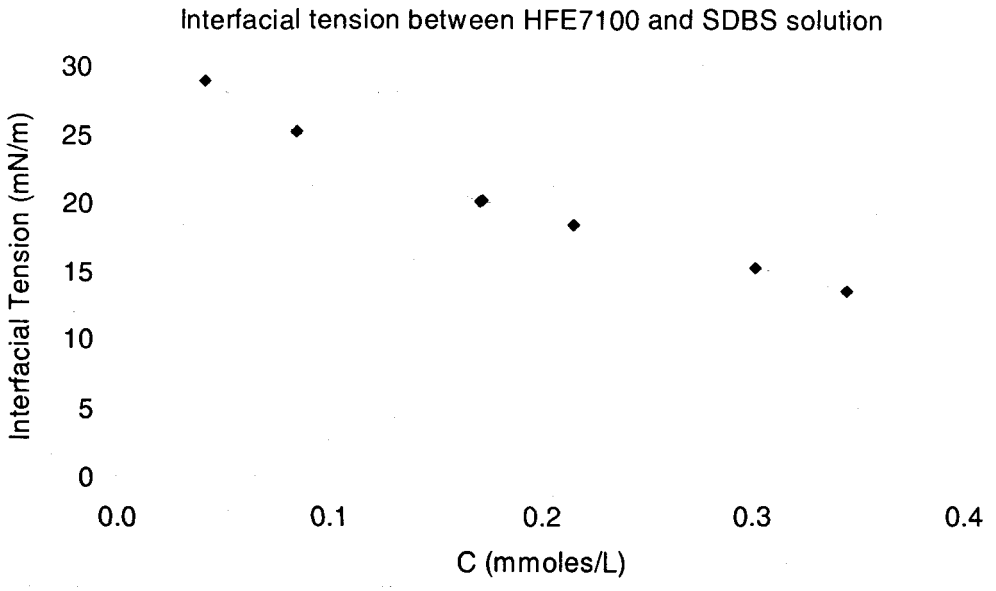

Figure 4-4a: Interfacial tension measured at various HFE7100-SDBS solution interfaces for SDBS solutions between 0-120 mg/L.

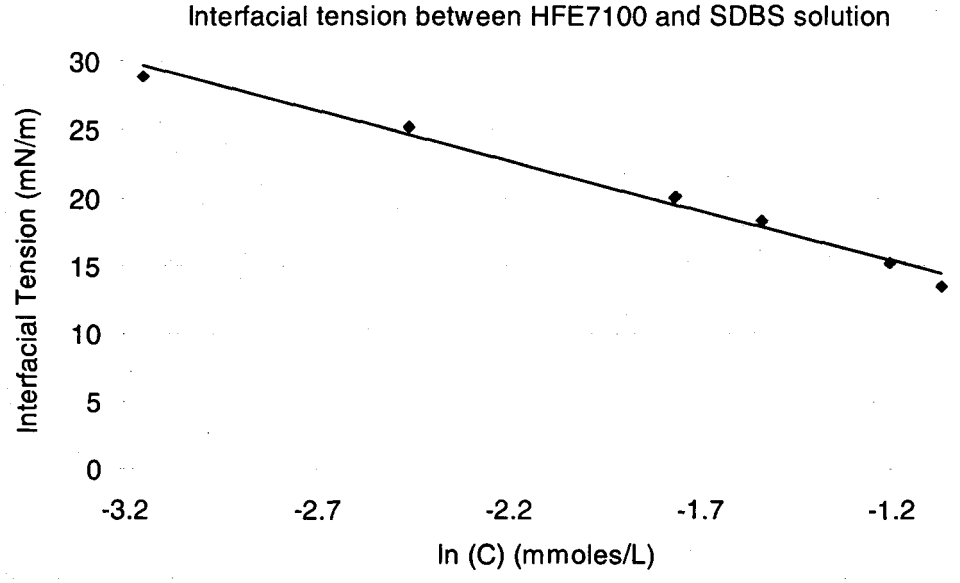

Figure 4-4b: Natural log plot of interfacial tension measured at various HFE7100-SDBS solution interfaces for SDBS solutions between 0-120 mg/L.

Table 4-4: Summary of regression fits to interfacial tension data for three DNAPL-SDBS solution plots (source: current Fisher Scientific MSDS sheets).

DNAPL	Tracer	ρ_{DNAPL} (g/mL)	R^2	β
HFE7100 (synthetic, methyl nonafluorobutyl ether)	SDBS	1.5	0.98	7.32
Tetrachloroethylene (PCE)[a]	SDBS	1.62	0.98	12.28
FC-40 oil (an inert, synthetic fluorocarbon)[a]	SDBS	~1.9	0.98	5.34

[a] data from Kim et al., 1999

4.3.2. Background Sorption of SDBS

Because the interfacial area calculations are based on the retardation of SDBS due to sorption at the fluid-fluid interfaces, it was also important to estimate the SDBS sorption to other materials in the experimental set-up aside from the fluid-fluid interfacial area. In order to determine whether SDBS adsorbed to the fracture cast and apparatus, an interfacial tracer test was conducted in each fracture in the absence of HFE7100. A pulse of SDBS solution of known SDBS concentration and volume was sent through each fracture at a known flow rate. A mass balance was performed to determine the mass of SDBS lost to the system.

Background tracer tests performed prior to the interfacial tracer tests produced a large SDBS adsorption in the range of 25 %. This is largely a result of a number of available adsorption sites in the system as no other tracer test had been performed. Subsequent losses were in the range of 5 %, which implies that SDBS was close to saturating the available sorption sites within the system. Although a dilute bleach solution

was pumped through the system between experiments, SDBS appears to have remained adsorbed to the system likely because of its low aqueous solubility. Assuming that the SDBS remained adsorbed to the system, the background SDBS adsorption was considered negligible.

4.3.3. Tracer Breakthrough Curves

All of the interfacial tracer tests were conducted with an influent SDBS concentration between 27.2 mg/L and 42.1 mg/L (0.08 to 0.12mM), which is much lower than the CMC of 418 mg/L (1.2mM). The low influent SDBS concentrations were necessary for maintaining the entrapped HFE7100 morphology. Preliminary experiments conducted at SDBS concentrations in the range of 300mg/L resulted in HFE7100 mobilization due to decreased interfacial tensions. The low influent SDBS concentrations are sufficient to provide the required data for interfacial area calculations since Kim and associates (1999) found that the calculated a_{nw} values for a DNAPL-water interface was fairly consistent over a wide range of SDBS influent concentrations (0.03-2.2mM). In fact, a low influent SDBS concentration minimizes the surface tension change during displacement experiments (Kim et al., 1997), which is an advantage as it maintains the water content and DNAPL morphology.

The breakthrough curves (BTCs) for the three interfacial tracer tests are provided in Figures 4-5a through 4-5c, where SDBS acted as the reactive tracer and acid yellow 17 acted as the non-reactive tracer. The BTCs for all experiments indicated a retardation of

SDBS due to the existence of the DNAPL-water interface (Figure 4-5a through 4-5c). The measured effluent tracer concentrations were normalized using the average influent concentration listed in Table 4-4, after which they were adjusted to reflect the concentration exiting the fracture plane using (4-3). Again, the BTCs display significantly more variability than the raw breakthrough curves provided in Appendix D. This variability can be attributed in part to error from the application of (4-3) because the derivative magnifies small variations in the temporal slope of the raw data.

More importantly, the variability in the BTCs is a result of the preferred flow pathways for tracer transport along a discrete fracture plane in the presence of the entrapped HFE7100. Because fractures 1 and 2 had relatively low tracer aperture ratios, it is expected that the tracer flow path has high variability. The flow pathway is not only dependent on the aperture field variability, it also depends on the connectivity between void spaces along the fracture plane. In addition, under a given hydraulic gradient, small aperture regions will conduct fluid at higher velocities than large aperture regions. Therefore the tracer solution flowing through a number of connected small aperture regions will reach the effluent end of the fracture before tracer solution migrating through larger aperture regions.

In addition, the presence of the entrapped HFE7100 influences the tracer solution pathway. Because entrapped HFE7100 is immiscible in water, the tracer solution must move around the HFE7100 mass entrapped in the fracture plane. A large HFE7100 blob

would prevent the tracer solution from passing, until it reached the outer edges of the blob where it could pass by. As a result, both the fracture plane characteristics and the presence of the entrapped HFE7100 influence the variability of the tracer concentrations measured at the effluent end of the fracture plane.

The BTCs also display what is commonly referred to as the tailing effect, where normalized SDBS concentrations take a long time to reach unity or equilibrium. This effect has been observed in a number of porous media studies (Annable et al., 1998; Kim et al., 1999; Dai et al., 2001) and is likely a result of spatial heterogeneities of the system, spatial distribution of the entrapped HFE7100, and non-equilibrium adsorption. Because the variable aperture fracture system is highly heterogeneous, and so too is the entrapped HFE7100, it is not surprising to observe extensive tailing in the BTCs.

The influent concentration measured periodically during the tracer tests, varied slightly over time. The same trend was observed during the acid yellow 17 tracer tests described in Section 4.1.2., where the influent concentrations took some time to stabilize. Again, this indicates that the recirculation system is not mixing the influent solution efficiently, which may be due to blockages in the re-circulation system or in the method employed in the tracer test to achieve a uniform initial tracer concentration.

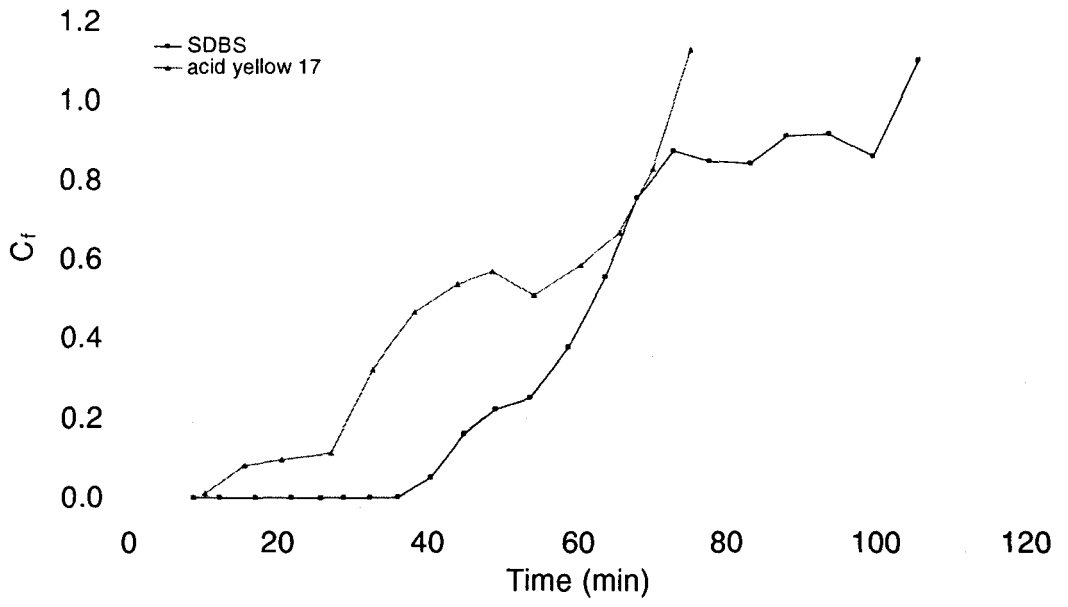

Figure 4-5a: BTCs for SDBS (reactive) and acid yellow 17 (non-reactive) tracers in fracture 1 experiment 1.

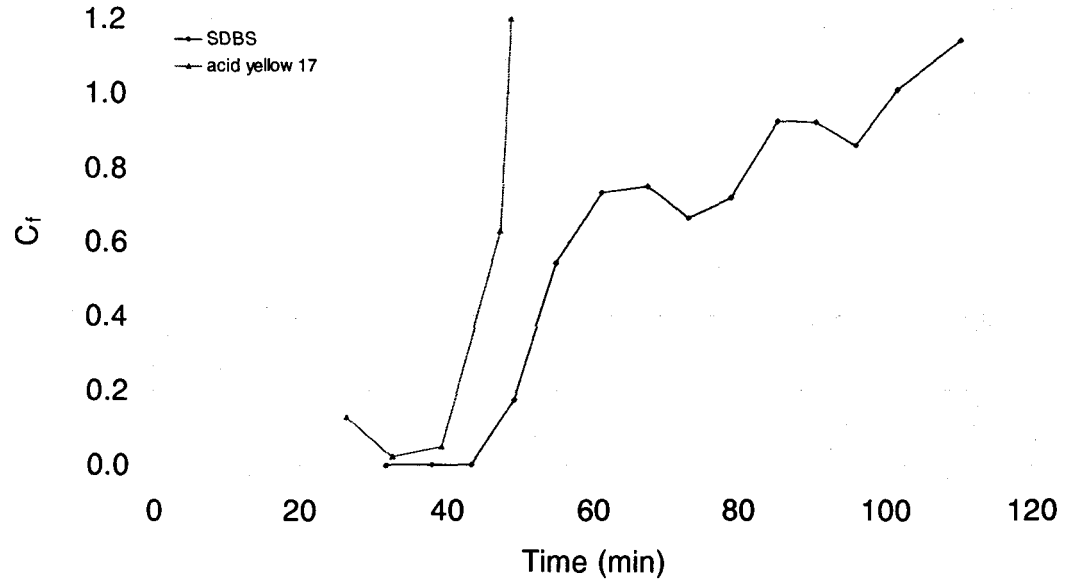

Figure 4-5b: BTCs for SDBS (reactive) and acid yellow 17 (non-reactive) tracers in fracture 1 experiment 2.

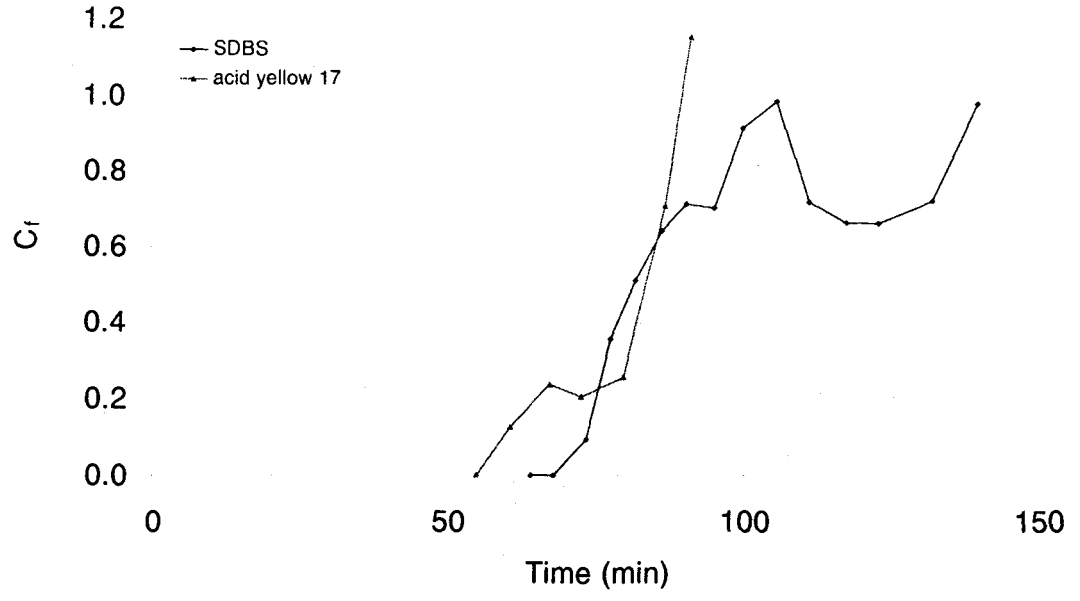

Figure 4-5c: BTCs for SDBS (reactive) and acid yellow 17 (non-reactive) tracers in fracture 2 experiment 3.

4.3.4. Specific DNAPL-Water Interfacial Area, a_{nw}

The specific HFE7100-water interfacial area, a_{nw} for each experiment was calculated from the retardation factor, R_{if}, obtained from the moment analysis of the reactive and non-reactive tracer BTCs using (2-13). For each experiment, the flow rate, Q was within the valid range of specific discharge for laminar flow, which is indicative of negligible inertial forces. The experimental conditions for each a_{nw} value are reported in Table 4-5. The θ_w was calculated from the volume of HFE7100 entrapped (V_H) and the fracture volume (V_F) where $\theta_w = V_F - V_H / V_F$.

Table 4-5: Summary of parameters for interfacial tracer experiments.

Exp No.	Fracture	Q (mL/min)	C_o (mg/L)	R_{ift} (-)	θ_w (-)	K_i (10^{-3}cm)	a_{nw} (cm^2/cm^3)	H_N (cm^2/cm^3)
1	Fracture 1	0.60	42.1	1.4	0.38	1.23	133	2.4
2	Fracture 1	0.65	38.6	1.8	0.48	1.33	291	5.9
3	Fracture 2	2.43	27.2	1.1	0.80	1.88	83	4.2

Although a similar HFE7100 mass was entrapped in fracture 1 in experiments 1 and 2 (62 % and 52 % respectively), the a_{nw} values differ by 54%, which is a result of the different morphologies of the trapped HFE7100 (Figure 4-3a, 4-3b). In experiment 1, a large DNAPL blob was entrapped, which analogous to a DNAPL pool in unconsolidated porous media; in experiment 2, a large number of small HFE7100 blobs were entrapped all across the fracture plane in a heterogeneous DNAPL distribution. Both cases showed measurable retardation, which was used to calculate the a_{nw} values for each occurrence. The a_{nw} values were 133 cm^2/cm^3 for the HFE7100 pool and 291 cm^2/cm^3 for the heterogeneously distributed HFE7100. These results are expected considering that experiment 2 had a larger surface area to volume ratio, otherwise known as the morphology index, H_N.

The entrapped HFE7100 distribution in experiment 3 (fracture 2) had a small number of HFE7100 blobs, which were also heterogeneously distributed, yet more similar to a residual DNAPL configuration in porous media due to the low DNAPL saturation. A small retardation factor was obtained from which an a_{nw} value of 83 cm^2/cm^3 was calculated. Although experiment 3 had a low HFE7100 saturation (20%), it

had a high morphology index, H_N, indicating that the HFE7100 entrapped in fracture 2 had a large surface area to volume ratio.

4.3.5. Verification of a_{nw} Through Visualization

Because the interfacial tracer technique has not been applied in fractured systems to date, there are no existing data with which the results of this work can be compared. Therefore, a verification method using digital image software was employed to obtain an interfacial area comparable to the experimental value. This verification method was possible since the fracture casts were fabricated from a transparent epoxy material. The interfacial areas obtained from the digital photo analysis, expressed as the interfacial area per volume of the system, were compared to the experimental interfacial areas (Table 4-6).

Table 4-6: Summary of interfacial areas obtained using the digital image software and compared to the experimental interfacial areas.

Exp. No.	Fracture	No. of blobs	Interfacial area from photo(cm^2)	Fracture volume (cm^3)	a_{nw} from photo (cm^2/cm^3)	a_{nw} experimental (cm^2/cm^3)	% error
1	Fracture 1	46	6,693	45	157	133	4
2	Fracture 1	128	12,331	45	275	291	10
3	Fracture 2	105	8,912	181	73	83	12

*interfacial area from photo was calculated using the e_{mb}

The a_{nw} values obtained through digital photo analysis compared well with the interfacial area values based on surfactant adsorption technique since all experimental a_{nw} values were within 12 % error of the verification a_{nw} values.

4.3.6. Possible Reasons for the Small Discrepancies

A number of factors may contribute to the discrepancies between the experimental a_{nw} and verification a_{nw}. The errors introduced from the experimental method are largely a result of the accessibility of the tracer solution to the entrapped HFE7100 mass and the heterogeneity of the fractured rock system. As a result, the values reported in Table 4-4 may not necessarily represent the total HFE7100-water interfacial area. The tracer solution may bypass the HFE7100-water interface in a number of situations. For instance, in highly heterogeneous HFE7100 distributions, small or miniscule HFE7100 blobs may be located in regions excluded from the main tracer flow path, or they may be located behind larger HFE7100 blobs along the tracer flow path, in which case, the tracer solution could sidestep them (Figure 4-6a). Moreover, dead zones caused by large asperities that pinch the fracture closed along the tracer flow path, completely isolating HFE7100-water interfaces from the tracer solution (Figure 4-6b). In fact, it is quite probable that only those HFE7100-water interfaces exposed along the main mobile water domain were accounted for in the a_{nw} values.

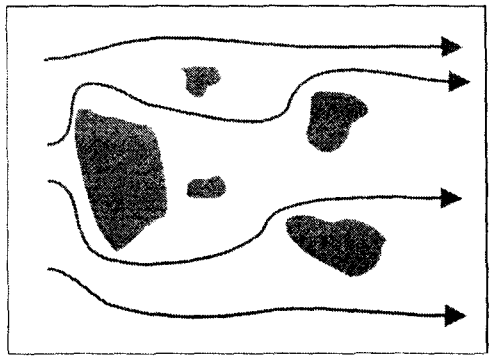

Figure 4-6a: Tracer flow (arrows) that by-passes small HFE7100 blobs (grey patches) along the flow path.

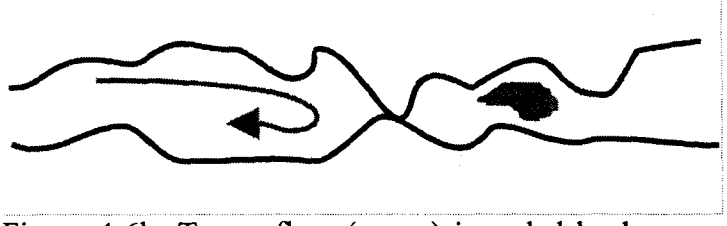

Figure 4-6b: Tracer flow (arrow) impeded by large asperities along the fracture plane, thereby preventing contact with the HFE7100 blob trapped behind asperity (grey patch).

The heterogeneity of the system also influences the tracer flow path, and therefore can influence the a_{nw} values. As noted in the DNAPL entrapment experiments, there is a preferred path of flow along a variable aperture fracture. As a result, the tracer solution likely travelled along the preferred pathway, which may or may not have included the majority of HFE7100-water interfaces. For these reasons, the experimental approach employed in this study provides a measure of the effective hydrodynamically accessible HFE7100-water interfacial area.

A number of factors contribute to the variation between the percent error in each experiment. The percent error in experiment 2 was higher than in experiment 1 (10 % and

4% respectively) even though they were performed on the same fracture. This is likely a result of the different HFE7100 entrapment configurations. Experiment 2 had a number of HFE7100 blobs, heterogeneously distributed, which introduces a number of possible errors in the calculation of the verification a_{nw} value. Tracing a large number of small blobs in the Image Tool software is difficult since the tracing feature does not lend itself to miniscule circle shapes, nor are the boundaries of these small blobs as clear when the image is enlarged. Small HFE7100 blobs located near the fracture plane boundaries may have been omitted since the colour contrast between the red-dyed water and colourless HFE7100 was low in these areas. In addition, it is possible that through human error some of the small blobs were missed, although labelling of HFE7100 blobs was meant to minimize this source of error.

The 12 percent error observed in experiment 3 may also be attributed to errors in the verification a_{nw} value resulting from a heterogeneous HFE7100 configuration, although the different characteristics of fracture 2 may play a role. Because fracture 2 was a cast of a natural granite fracture, it had aperture geometries that were very angular compared to fracture 1 which was a cast of a limestone fracture. In addition, fracture 2 had a smaller aperture ratio than fracture 1, which implies that it had a larger variation of apertures across the fracture plane. These characteristics may have influenced the percent error observed in experiment 3 since the actual HFE7100-water interface may not have been well represented in the plan-view digital photo used to determine the verification a_{nw}. For instance, if a HFE7100 blob was trapped as a prism shape, the plan-view digital

photo would only show the tip of the prism. In this case, the verification a_{nw} would have been underestimated.

Nevertheless, the method used to obtain the verification a_{nw} value appears valid since the results corroborate a conceptual model developed by Parker and associates (1994) for immiscible phase organic liquids in fractured porous media. The model developed by Parker and associates (1994) postulated that, due to the relative wetting properties of DNAPL and water with respect to rock, a thin layer of water exists between trapped DNAPL and the fracture wall. Although this thin layer of water was not visible in the visualization experiments, it was encountered in the a_{nw} calculations from the image analysis. Due to the small degree of error between the interfacial tracer test and image analysis techniques, it seems that this thin film of fluid is, in fact, present.

Not only does the calculation of the verification a_{nw} value validate the conceptual model developed by Parker and associates (1994), the percent error in the measured a_{nw} was much lower than those typically derived from traditional point measurement techniques (e.g. core sampling, cone penetrometer testing, and geophysical logging) used in unconsolidated porous media. In all likelihood these traditional point measurements can easily bypass the DNAPL source zone entirely resulting in a 100 % error. In comparison, the interfacial tracer technique developed for fractured rock systems produced a small degree of error between the measured a_{nw} and the verification a_{nw} for two different systems. Together, these facts imply that the interfacial tracer technique

developed for fracture rock systems is a valid approach for estimating the interfacial area between two immiscible fluids.

CHAPTER 5.0 CONCLUSIONS

The conclusions from the key objectives of this research, specifically the aperture field characterization, DNAPL entrapment, interfacial tracer technique and verification of the experimental a_{nw}, are provided in the following sections.

5.1. APERTURE FIELD CHARACTERIZATION

Based on the hydraulic and tracer studies, three aperture values e_f, e_{mb} ,e_h were determined for two fractures in the valid region of specific discharge. For both fracture 1 and 2 the relationship between the three apertures was: $e_{mb}>e_h>e_f$, which agrees well with aperture relationships reported in the literature (Tsang, 1992; Dickson, 2003; Brush, 2000). The tracer aperture ratio, δ for each fracture indicated that fracture 2 had a larger range of extreme aperture regions compared to fracture 1. This finding was in agreement with visual observation of the two fractures where fracture 2 appeared much more undulous than fracture 1.

5.2. DNAPL ENTRAPMENT EXPERIMENTS

The two fracture casts developed for the visualization experiments were successfully fabricated since each fracture face mirrored those of the natural fracture plane, and when the fracture faces were mated the fracture opening was the same in size and shape as the natural fracture plane. The dynamic processes observed as HFE7100 was emplaced included: (1) the HFE7100 pinched off due to decrease in capillary

pressure upon entering a larger aperture region; and, (2) the HFE7100 exited the fracture plane along a preferred pathway.

The HFE7100 trapped in experiment 1 and 3 were entrapped under flushing capillary numbers, N_c on the order of 10^{-5}. This is consistent with results presented by Dickson (2001). The N_c value is not particularly meaningful for experiment 2 due to the presence of gravitational forces. The configuration of HFE7100 in each experiment was as follows:

- In experiment 1, a large HFE7100 blob was entrapped analogous to a high saturation (>20 % saturation) DNAPL pool in unconsolidated porous media.
- In experiment 2, a large number of small HFE7100 blobs were entrapped across the fracture plane representative of a high saturation (>20 % saturation) heterogeneous DNAPL distribution.
- In experiment 3, a small number of HFE7100 blobs were entrapped, which is analogous to a residual distribution (<20% saturation) in unconsolidated porous media.

5.3. INTERFACIAL TRACER TECHNIQUE

The preliminary data necessary for the immiscible fluid-fluid interfacial area, a_{nw} included the SDBS adsorption distribution coefficient K_i and the background SDBS adsorption. The key conclusions from these preliminary tests are as follows:

- The K_i values were determined through interfacial tension measurements of HFE7100-SDBS solutions. The data showed an exponential decrease in interfacial tension with increasing SDBS concentration, which is consistent with results reported in the literature (Kim et al, 1999; Saripally et al, 1998; Annable et al., 1998). The regression fit of a log plot of the data produced a slope ($d\gamma/dC$) that was in agreement with reported values for interfacial tension data for two similar DNAPL-SDBS solutions (Kim et al., 1999).
- After running a series of background SDBS tracer tests, SDBS appeared to saturate the sorption sites available in the experimental system. Subsequent losses were in the range of 5% and were considered negligible.

5.4 SPECIFIC DNAPL-WATER INTERFACIAL AREA, a_{nw}

The a_{nw} values, calculated using the Gibbs adsorption isotherm for each experiment were in agreement with the visual observations of each HFE7100 configuration. The conclusions from the interfacial tracer experiments are as follows:

- All interfacial tracer experiments indicated a retardation of SDBS in the breakthrough curve (BTC) due to the existence of the HFE7100-water interface.
- The BTCs displayed significant variability which could be attributed to: (1) error from correcting the concentrations in the mixing cell using (4-3), (2) spatial heterogeneities of the system and spatial distribution of the entrapped HFE7100, which influence tracer transport, and (3) non-equilibrium adsorption.
- The a_{nw} values were 133 cm^2/cm^3 for the HFE7100 pool in experiment

1 and 291 cm^2/cm^3 for the heterogeneously distributed HFE7100 in experiment 2. The larger a_{nw} in experiment 2 was expected as the DNAPL was trapped in a large number of smaller blobs than it was in experiment 1, and therefore had a larger interfacial area.

- Because experiment 2 had a greater H_N than experiment 1, the HFE7100 had good contact with the aqueous phase, thereby increasing the potential for inter-phase mass transfer.
- The a_{nw} value for experiment 3 was 83 cm^2/cm^3 for a heterogeneous residual HFE7100 configuration saturation (20% saturation), however, it had a relatively high H_N compared to experiment 1 and 2 owing to a small HFE7100 volume entrapment, which corresponds to a relatively high interfacial area to volume ratio, and therefore relatively high mass transfer rates.
- The a_{nw} values represent the effective hydrodynamically accessible HFE7100-water interfacial area only since the a_{nw} values are limited by the accessibility of the tracer solution to the entrapped HFE7100 mass.
- Error in the a_{nw} values may have been introduced through: (1) whether HFE7100 blobs were located along the preferred flow path, (2) small HFE7100 blobs hidden behind larger ones in the direction of tracer flow, (3) dead zones caused by large asperities that pinch the fracture closed isolating the tracer solution from the HFE7100-water interfaces.

5.5. VERIFICATION OF THE EXPERIMENTAL a_{nw}

The a_{nw} values obtained through digital photo analysis compared well with the interfacial area values based on the surfactant adsorption technique since all experimental a_{nw} values were within 12 % error of the verification a_{nw} values. The main conclusions include:

- The % error in experiment 2 was higher than in experiment 1 (10 % and 4% respectively) even though they were performed on the same fracture, which was likely a result of the different HFE7100 configurations. A more heterogeneous distribution of HFE7100 in experiment 2 was likely subjected to more error in both the experimental a_{nw} and the verification a_{nw} calculation.
- The 12 % error observed in experiment 3 likely resulted from a heterogeneous HFE7100 configuration and the fracture cast characteristics. Fracture 2 was a cast of a natural granite fracture, having angular apertures and a larger aperture ratio, which likely trapped HFE7100 not captured in the plan-view photo used to determine the verification a_{nw} value.
- The error introduced in the verification a_{nw} value may be attributed to: (1) inaccurate tracing of small blob circumference due to software limitations and human error, (2) exclusion of small blobs through human error, especially those located near the fracture plane boundaries where the colour contrast between the red-dyed water and colourless HFE7100 was low.

- The verification a_{nw} may have overestimated the total blob surface area since it assumes that all blob heights were equal to the mass balance aperture, which is not the case for blobs located in small aperture regions.
- Because the verification a_{nw} incorporated the entire blob surface area, the verification method validated the conceptual model developed by Parker and associates (1994), who postulated that a thin film of water existed between the blob and fracture wall.
- The percent error was much lower than error observed using traditional point measurement techniques (e.g. core sampling, cone penetrometer testing, and geophysical logging), where the potential to bypass DNAPL source zones is large, resulting in a 100% error.

5.6. RECOMMENDATIONS

While the interfacial tracer technique was only applied to two unique fractures in this study, it demonstrates the ability to obtain a measure of the DNAPL-water contact area, and offers an additional tool for the characterization of DNAPL source zones. However, further testing is required to validate this technique. Recommendations for future work include more systematic and comprehensive lab experiments that include a wider range of DNAPLs and interfacial tracers, a variety of hydrologic and geochemical environments, and a variety of DNAPL surface area to volume ratios.

In addition, by performing the interfacial tracer test in tandem with the partitioning tracer test, two measures of the DNAPL source zone could be obtained, including the DNAPL interfacial area, a_{nw} and DNAPL saturation, S_N. Although the DNAPL saturation employed in this thesis was based on the volume of DNAPL entrapped in the fracture, a more accurate measure of DNAPL saturation may be obtained through the partitioning tracer test, which is comparable to the interfacial area obtained through the interfacial tracer test and therefore provides a more accurate DNAPL morphology index, H_N. The ability to determine the variation in the DNAPL-water contact area, in addition to the spatial distribution of the DNAPL content significantly enhances our understanding of contaminated sites. By employing both the interfacial tracer test and partitioning test, scientists can better characterize DNAPL source zones in fracture rock systems.

Once the interfacial tracer technique has been tested in a variety of HFE7100 morphologies and hydrogeological settings at the lab scale, the interfacial tracer technique, preferably along with the partitioning tracer technique, may be applied to the field in discrete fractured rock systems. In doing so, we hope to establish that the tracer tests are in fact providing reliable absolute measures of DNAPL source zones, including DNAPL content, distributions and water contact area. This type of information is needed for risk assessment, better design of site remediation efforts, and for assessment of remediation technology performance.

6.0 REFERENCE LIST

Annable, M.D., Jawitz, J.W., Rao, P.S.C., Dai, D.P., Kim, H., and A.L. Wood. 1998a. *Field Evaluation of Interfacial and Partitioning Tracers for Characterization of Effective NAPL-Water Contact Areas*. Groundwater. V36 (3), pp 495-502.

Annable, Michael D., Rao, P. Suresh, Kim, Heonki, and K. Prasad Saripalli. 1998b. *Response to Comment on "Estimation of Nonaqueous Phase Liquid-Water Interfacial Areas in Porous Media following Mobilization by Chemical Flooding"*. Environmental Science Technology. V32 (23), pp3838-3839.

Annable, Michael D., Rao, P.S.C., Hatfield, Kirk, Graham, Wendy D., Wood, A.L., and C.G. Enfield. 1998c. *Partitioning Tracers for Measuring Residual NAPL: Field-Scale Test Results*. Journal of Environmental Engineering. pp498-503.

Brush, D.J.2000. *Three-dimensional fluid flow and solute transport in rough-walled fractures*. Ph.D. Dissertation, Department of Civil Engineering, University of Waterloo, Waterloo, ON.

Brush, D.J. and N.R.Thomson. 2003. *Fluid flow in synthetic rough-walled fractures: Navier-Stokes, Stokes, and local cubic law simulations*. Water Resources Research. V39(4), (SBH), pp 5-1 to 5-15.

Cain, R. Brent, Johnson, Gwynn R., McCray, John E., Blanford, William J., and Mark L. Brusseau. 2000. *Partitioning Tracer Tests for Evaluating Remediation Performance.* Groundwater. V38(5), pp752-761.

de Marsily, G. 1986. *Quantitative Hydrogeology: Groundwater Hydrology for Engineers.* Academic Press, Toronto, ON.

Davis, B.M., Istok, J.D., and L. Semprini. 2002. Push-pull partitioning tracer tests using radon-222 to quantify non-aqueous phase liquid contamination. Journal of Contaminant Hydrology. (Article in press).

Deeds, Neil E., Mckinney, Deane C., and Gary A. Pope. 2000. *Laboratory characterization of non-aqueous phase liquid/tracer interaction in support of a vadose zone partitioning interwell tracer test.* Journal of Contaminant Hydrology. V41, pp193-204.

Delshad, M., Pope, G.A., and K. Sepehrnoori. 1996. *A compositional simulator for modeling surfactant enhanced aquifer remediation, 1 Formulation.* Journal of Contaminant Hydrology. V23, pp303-327.

Dickson S.E., 2001. *Dissolution of Entrapped DNAPLs in Variable Aperture Fractures.* PhD thesis at the University of Waterloo, Ontario.

Dickson, S.E. 2003. Dissolution of entrapped DNAPLs in variable aperture fractures: experimental data and empirical model. Environmental Science and Technology. Web release August 2003.

Dongping, Dai, Barranco Jr., Frank T., and Tissa H. Illangasekare. 2001. *Partitioning and Interfacial Tracers for Differentiating NAPL Entrapment Configuration: Column-Scale Investigation.* Environmental Science and Technology. V35, pp4894-4899.

Dullien, F.A.L.1979. *Porous Media: Fluid Transport and Pore Structure.* Academic Press, San Diego, CA.

Dwarakanath, Varadarajan and Gary A. Pope. 1998. *New Approach for Estimating Alcohol Partition Coefficients between Nonaqueous Phase Liquids and Water.* Environmental Science and Technology. V32, pp1662-1666.

Field, Jennifer A., and Jonathan D. Istok. 1998. *Comment on "Estimation of Nonaqueous Phase Liquid-Water Interfacial Areas in Porous Media following Mobilization by Chemical Flooding".* Environmental Science and Technology. V32 (23) pp3836-3837.

Fisher Scientific. 2004. MSDS Sheets for a variety of chemicals.

Freeze and Cheery 1979. *Groundwater.* Prentice Hall, Englewood Cliffs, New Jersey.

Gierke, John S., Sanders, Deborah L., and David L. Perram. 1999. *Laboratory Studies of Aqueous Partitioning Tracer Tests for Measuring Nonaqueous Phase Liquid Volumes.* Water Environment Research. V71(4), pp465-474.

Gvirtzman, H and Paul V. Roberts. 1991. *Pore Scale Spatial Analysis of Two immiscible Fluids in Porous Media.* Water Resources Research. V 27 (6), pp 1165-1176.

Healy, T.W., P.Somasundaran, and D.W. Fuerstenau. 2003. *The adsorption of alkyl and alkylbenzene sulfonates at mineral oxide-water interfaces.* International Journal of Mineral Processing. V72, pp3-10.

Hummel, D.O. 2000. *Handbook of Surfactant Analysis: Chemical, Physico-chemical and Physical Methods.* John-Wiley and Sons Ltd: Toronto, ON.

Istok, Jonathan D., Field, Jennifer A., Schroth, Martin, H., and *Varadarajan Dwarakanath. Single-Well "Push-Pull" Partitioning Tracer Test for NAPL Detection in the Subsurface.* Environmental Science Technology. V36, pp2708-2716.

Jawitz, James W., Sillan, Randall K., Annable, Michael D., Rao, P.Suresh C., and Kevin Warner. 2000. *In-Situ Alcohol Flushing of a DNAPL Source Zone at a Dry Cleaner Site.* Environmental Science and Technology. V34(17), pp3722-3729.

Jin, Minquan, Delshad, Mojdeh, Dwarakanath, Varadarajan, McKinney, Daene C., Pope, Gary A., Sepehrnoori, Kamy, and Charles E. Tilburg. 1995. *Partitioning tracer test for detection, estimation, and remediation performance assessment of subsurface nonaqueous phase liquids.* Water Resources Research. V31(5) pp1201-1211.

Jin, M., Butler, G.W., Jackson, R.E., Mariner, P.E., Pickens, J.F., Pope, G.A., Brown, C.L. and D.C. McKinney. 1997. *Sensitivity Models and Design Protocol for Partitioning Tracer Tests in Alluvial Aquifers.* Groundwater. V35(6), pp964-972.

Kueper, B.H. and D.B. McWhorter. 1991. *The behaviour of dense, non-aqueous phase liquids in fractured clay and rock.* Ground Water. V29(5), pp716-728.

Kim, Heonki and P. Suresh C. Rao. 1997. *Determination of effective air-water interfacial area in partially saturated porous media using surfactant adsorption.* Water Resources Research. V33(12), pp2705-2711.

Kim, Heonki, Michael D. Annable, and P. Suresh C. Rao. 1998. *Influence of Air-Water Interfacial Adsorption and Gas-Phase Partitioning on the Transport of Organic Chemicals in Unsaturated Porous Media.* Environmental Science Technology. V32, pp1253-1259.

Kim, H., Rao, P. Suresh C. and M.D. Annable. 1999. *Consistency of the interfacial tracer technique: experimental evaluation.* Journal of Contaminant Hydrology. V 40, pp 79-94.

Konzuk, J.S. and B.H. Kueper. 2004. *Evaluation of cubic law based models describing single-phase flow through a rough-walled fracture.* Water Resources Research. V40 (W02402).

Longino, B.L., 1998. *Residual non-wetting phase formation and mobilization in rough-walled fractures.* Ph.D. Dissertation, Department of Civil Engineering, Queen's University Kingston, ON.

Longino, B.L., and B.H. Kueper. 1999. *Nonwetting phase retention and mobilization in rock fractures.* Water Resources Research. V35 pp2085-2093.

Noordman, Wouter H., De Boer, Geert J., Wietzes, Pieter, Volkering, Frank and Dick B. Janssen. 2000. *Assessment of the Use of Partitioning and Interfacial Tracers To Determine the Content and Mass Removal Rates of Nonaqueous Phase Liquids.* Environmental Science Technology. V34 pp4301-4306.

Parker, B.L., R.W. Gillham and J.A. Cherry. 1994. Diffusive disappearance of immiscible phase organic liquids in fractured geologic media. Ground Water. V32(4) pp805-820.

Powers, Susan E., Loureiro, Celso O., Abriola, Linda M., and Walter J. Weber, Jr. 1991. *Theoretical Study of the Significance of Nonequilibrium Dissolution of Nonaqueous Phase Liquids in Subsurface Systems.* Water Resources Research. V 27 (4), pp 463-477.

Rao, P.S.C., Annable, M.D., Kim, H. and K.P. Saripalli. 1998. *Tracer techniques for site characterization and remediation technology performance assessment: recent developments and applications.* Groundwater Quality: Remediation and Protection (Proceedings of the GQ'98 Conference held at Tübingen, Germany, September 1998). IAHS Publ. no.50.

Rao, P. Suresh C., Annable, Michael D., and Heonki Kim. 2000. *NAPL source zone characterization and remediation technology performance assessment: recent developments and applications of tracer techniques.* Journal of Contaminant Hydrology. V 45, pp63-78.

Reeves, Paul C., and Michael A. Celia. 1996. *A functional relationship between capillary pressure, saturation, and interfacial area as revealed by a pore-scale network model.* Water Resources Research. V 32 (8), pp 2345-2358.

Rosen, Milton J. 1978. *Surfactants and Interfacial Phenomena.* John Wiley and Sons: Toronto, ON.

Saripalli, K. Prasad, Annable, M. D., and P.S.C. Rao. 1997a. *Estimation of Nonaueous Phase Liquid-Water Interfacial Areas in Porous Media following Mobilization by Chemical Flooding.* Environmental Science Technology. V31, pp3384-3388.

Saripalli, K. Prasad, Kim, Heonki, Suresh, P., Rao, C., and Michael D. Annable. 1997b. *Measurement of Specific Fluid-Fluid Interfacial Areas of Immiscible Fluids in Porous Media.* Environmental Science and Technology. V 31 (3), pp 932-936.

Saripalli, K.Prasad, Rao, P.S.C., and M.D. Annable. 1998. *Determination of specific NAPL-water interfacial areas of residual NAPLs in porous media using the interfacial tracers technique.* Journal of Contaminant Hydrology. V 30, pp 375-391.

Schwille, F. 1988. *Dense Chlorinated Solvents in Porous and Fractured Media.* Lewis, New York.

Snow, D.T. 1965. A parallel plate model of fractured permeable media, Ph.D. thesis, University of California, Berkeley.

Tsang, Y.W. 1992. *Usage of "Equivalent Apertures" for Rock Fractures as Derived From Hydraulic and Tracer Tests.* Water Resources Research. V 28 (5), pp1451-1455.

Walter, J. Weber, Jr. and Francis A. DiGiano. 1996. *Process Dynamics in Environmental Systems*. John Wiley and Sons Inc.: New York, NY.

Wilson, Clinton S., Pau, Oliver, Pedit, Joseph A., and Cass T Miller. 2000. *Mass transfer rate limitation effects on partitioning tracer tests*. Journal of Contaminant Hydrology. V45, pp79-97.

Wise, William R., Dai, Dongping, Fitzpatrick, Elizabeth A., Evans, Lalenia W., Rao, P. Suresh C., and Michael D. Annable. 1999. *Non-aqueous phase liquid characterization via partitioning trace tests: a modified Langmuir relation to describe partitioning nonlinearities.* Journal of Contaminant Hydrology. V36, pp153-165.

WHO. 1996. *Guidelines for drinking-water quality*. Health criteria and other supporting information. Geneva. World Health Organization. 2nd ed. Vol. 2.

Zhang, Yan and Wendy D. Graham. 2001. *Partitioning tracer transport in a hydrogeochemically heterogeneous aquifer.* Water Resources Research. V37 (8), pp2037-2048.

APPENDIX A: CALIBRATION DATA

Table A1: Tipping bucket rain gauge calibration data.

	Tipping volume (mL/tip)	
	Rain Gauge 1	Rain Gauge 2
	5.1	4.9
	5.2	4.8
	4.9	5.3
	5.0	5.0
	5.0	5.1
	4.8	5.2
	5.2	4.9
	5.1	5.0
	5.0	4.9
Average (mL/tip):	5.0	5.0
Standard deviation (mL/tip):	0.12	0.15

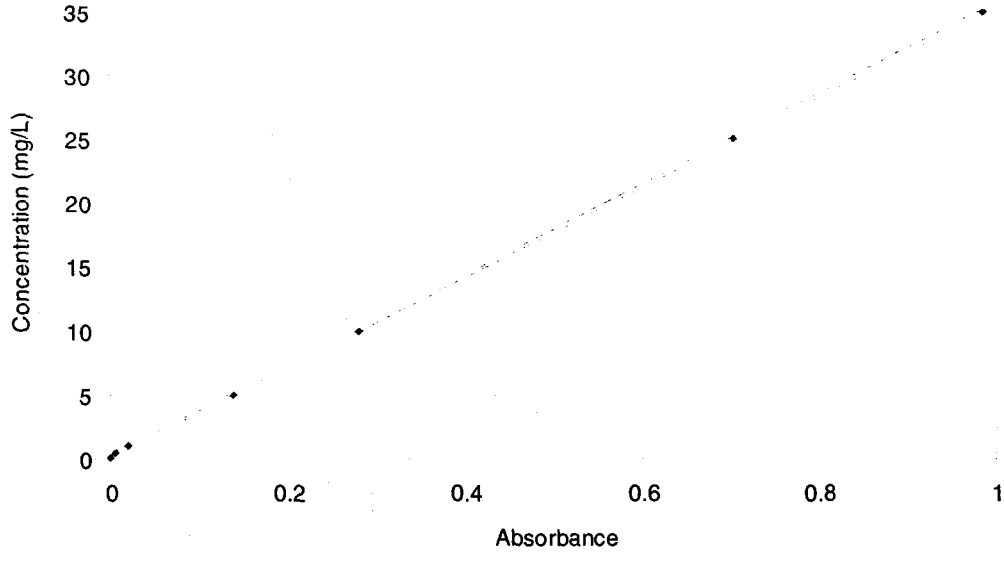

Figure A1: Standard curve for acid yellow 17 using the mass spectrophotometer at 400nm. The two dashed lines represent the line of best fit for the 95% confidence interval of the data. The R^2 value was 1 for the lower limit and 0.999 for the upper limit of the confidence interval.

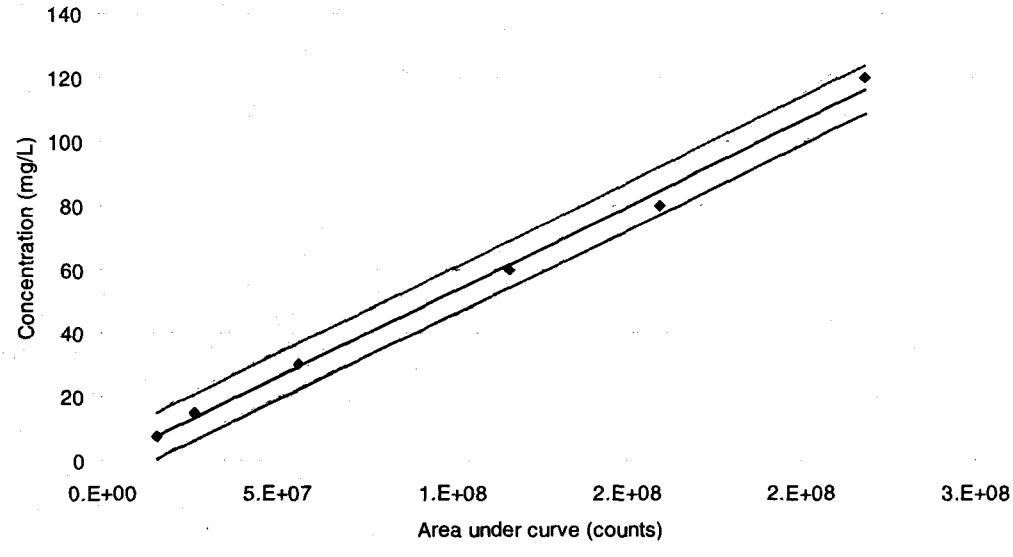

Figure A2: Standard curve for sodiumdodecylbenzenesulphonate (SDBS) using the HPLC followed by fluorescence detection. The two dashed lines represent the line of best fit for the 95% confidence interval of the data. The R^2 value was 0.996 for the lower limit and 0.995 for the upper limit of the confidence interval.

APPENDIX B: INTERFACIAL TENSION DATA

Table B2a: Interfacial tension data between HFE7100 and SDBS solution using the Drop Volume Method (Lauda IV). July to August, 2004.

Conc. (mg/L)	Run	Tension (mN/m)	V (uL)	t (s)	dt:0.065 s/uL	Mean Reproducibility of Singe Drops:
60.22	1	27.89 +/- 0.19	26.55	5.3 +/- 0.2		
*N=3x6	2	26.94 +/- 0.05	25.58	9.7 +/- 0.2	d(IT)/dt	Volume: +/- 0.07uL
	3	26.22 +/- 0.03	24.83	15.5 +/- 0.2	(mN/ms):	Stroke: +/- 1.7um
	4	25.66 +/- 0.10	24.26	20.9 +/- 0.7	-0.043	
	5	25.19 +/- 0.06	23.78	25.5 +/- 0.5	Correlation:	
	6	24.78 +/- 0.02	23.36	31.2 +/- 0.2	0.9862	
		22.24 +/- 0.05				
120.44	1	24.76 +/- 0.3	23.34	3.1 +/- 0.0	dt: 0.061s/uL	Mean Reproducibility of Singe Drops:
*N=3x13	2	23.25 +/- 0.05	21.81	5.7 +/- 0.1		
	3	21.94 +/- 0.02	20.47	9.0 +/- 0.1	d(IT)/dt	Volume: +/- 0.08uL
	4	20.9 +/- 0.06	19.43	12.9 +/- 0.2	(mN/ms):	Stroke: +/- 1.8um
	5	20.15 +/- 0.08	18.67	16.5 +/- 0.3		
	6	19.6 +/- 0.03	18.12	20.6 +/- 0.1		
	7	19.28 +/- 0.1	17.8	24.9 +/- 1.0		
	8	19.07 +/- 0.07	17.59	28.0 +/- 0.5		
	9	18.74 +/- 0.07	17.26	30.6 +/- 0.6	-0.055	
	10	18.50 +/- 0.07	17.01	33.7 +/- 0.9	Correlation:	
	11	18.32 +/- 0.05	16.83	37.3 +/- 0.5	0.9868	
	12	18.14 +/- 0.07	16.66	39.9 +/- 1.2		
	13	17.94 +/- 0.07	16.46	41.5 +/- 0.9		
		13.46 +/- 0.06				
60.22	1	27.54 +/- 0.09	26.19	4.9 +/- 0.3	dt:0.047 s/uL	Mean Reproducibility of Singe Drops:
*N=3x8	2	26.52 +/- 0.08	25.14	8.1 +/- 0.2		
	3	25.65 +/- 0.09	24.25	11.8 +/- 0.3	d(IT)/dt	Volume: +/- 0.09uL
	4	24.98 +/- 0.09	23.57	15.5 +/- 0.3	(mN/ms):	Stroke: +/- 2.2um
	5	24.56 +/- 0.13	23.13	19.1 +/- 0.5	-0.059	
	6	24.12+/- 0.14	22.69	23.1 +/- 0.9	Correlation:	
	7	23.88 +/- 0.12	22.44	26.4 +/- 1.1	0.9991	
	8	23.61 +/- 0.05	22.17	30.0 +/- 0.5		
		20.10 +/- 0.00				
75.28	1	25.74 +/- 0.34	24.35	4.4 +/- 0.6	dt: 0.053s/uL	Mean Reproducibility of Singe Drops:
*N=3x11	2	24.48 +/- 0.08	23.06	7.1 +/- 0.2		
	3	23.48 +/- 0.05	22.03	10.5 +/- 0.0	d(IT)/dt	Volume: +/- 0.12uL
	4	22.54 +/- 0.09	21.09	13.4 +/- 0.4	(mN/ms):	Stroke: +/- 2.9um
	5	21.91 +/- 0.06	20.45	17.3 +/- 0.4	-0.025	
	6	21.29 +/- 0.08	19.82	20.3 +/- 0.4	Correlation:	
	7	20.81 +/- 0.05	19.34	24.2 +/- 0.5	0.6973	
	8	20.27 +/- 0.16	18.74	25.2 +/- 1.4		
	9	20.04 +/- 0.20	18.56	31.7 +/- 1.9		
	10	20.21 +/- 0.16	18.73	36.3 +/- 1.6		
	11	20.17 +/- 0.18	18.69	37.2 +/- 2.0		
		18.24 +/- 0.62				

Table B2a continued: Interfacial tension data between HFE7100 and SDBS solution using the Drop Volume Method (Lauda IV). July to August, 2004.

Conc. (mg/L)	Run	Tension (mN/m)	V (uL)	t (s)		
105.39	1	25.47 +/- 0.24	24.06	3.8 +/- 0.2	dt:0.057s/uL	Mean Reproducibility of Singe Drops:
*N=3x12	2	24.17 +/- 0.05	22.74	6.6 +/- 0.3		
	3	23.04 +/- 0.09	21.59	10.3 +/- 0.2	d(IT)/dt	Volume: +/- 0.09uL
	4	22.16 +/- 0.06	20.7	13.6 +/- 0.2	(mN/ms):	Stroke: +/- 2.0um
	5	21.50 +/- 0.09	20.03	18.0 +/- 0.4	-0.051	
	6	20.96 +/- 0.06	19.49	21.4 +/- 0.4	Correlation:	
	7	20.56 +/- 0.03	19.08	25.5 +/- 0.3	0.9924	
	8	20.21 +/- 0.07	18.73	28.8 +/- 0.5		
	9	19.87 +/- 0.19	18.39	31.5 +/- 1.7		
	10	19.68 +/- 0.01	18.2	35.4 +/- 0.1		
	11	19.50 +/- 0.06	18.02	38.1 +/- 1.1		
	12	19.36 +/- 0.16	17.88	41.0 +/- 2.1		
		15.12 +/- 0.04				

Parameters programmed into tensiometer

Mode:	DYN	Dynamic
Svol:	5.0mL	syringe volume (containing HFE7100)
r:	1.050mm	radius of syringe tip
d:	0.500g/mL	density difference between two fluids (HFE7100 & SDBS solutions)
T:	25oC	Temperature
N:	3x11	3 samples; 11 runs (exceptions listed in table)
t:	0.04-0.40 (s/uL)	time allowed for drop to fall

Note: Values reported in bold were employed in Figure 4-4 and were derived by extrapolating the last 5.

Table B2b: Interfacial tension data between HFE7100 and SDBS solution using the Drop Volume Method (Lauda IV). May 2004.

Conc. (mg/L)	Run	Interfacial Tension (mN/m)	V (uL)	t (s)	dt: 0.036 s/uL	Mean Reproducibility of Singe Drops:
15	1	33.68 +/- 0.55	32.58	2.5 +/- 0.2		
	2	32.79 +/- 0.15	31.65	6.3 +/- 0.1	d(IT)/dt	Volume: +/- 0.00uL
	3	32.26 +/- 0.2	31.09	11.2 +/- 0.5	(mN/ms):	Stroke: 0.0um
	4	31.92 +/- 0.21	30.73	15.0 +/- 0.8	-0.022	
	5	31.60 +/- 0.25	30.40	18.4 +/- 0.9	Correlation:	
	6	31.33 +/- 0.11	30.12	21.6 +/- 0.6	0.9535	
	7	31.11 +/- 0.02	29.89	25.6 +/- 0.2		
	8	30.91 +/- 0.2	29.68	29.3 +/- 1.2		
	9	30.78 +/- 0.29	29.55	32.0 +/- 1.8		
	10	30.69 +/- 0.19	29.45	35.6 +/- 1.1		
	11	30.70 +/- 0.21	29.47	39.7 +/- 0.9		
		28.87 +/- 0.09				
30	1	31.00 +/- 0.23	29.78	2.0 +/- 0.2	dt: N/A s/uL	Mean Reproducibility of Singe Drops:
	2	29.50 +/- 0.21	28.22	4.4 +/- 0.2		
	3	28.64 +/- 0.15	27.33	9.0 +/- 0.2	d(IT)/dt	Volume: +/- 0.17uL
	4	28.15 +/- 0.12	26.82	13.0 +/- 0.5	(mN/ms):	Stroke: 2.0um
	5	27.70 +/- 0.21	26.36	16.2 +/- 0.9	-0.024	
	6	27.33 +/- 0.12	25.98	18.9 +/- 0.5	Correlation:	
	7	26.98 +/- 0.37	25.62	21.5 +/- 1.8	0.875	
	8	27.00 +/- 0.11	25.64	25.7 +/- 0.9		
	9	26.86 +/- 0.07	25.5	27.8 +/- 0.3		
	10	26.72 +/- 0.14	25.35	30.1 +/- 0.9		
	11	26.63 +/- 0.22	25.26	32.9 +/- 1.8		
		25.12 +/- 0.21				
60	1	29.88 +/- 0.41	28.62	1.8 +/- 0.0	dt: 0.030 s/uL	Mean Reproducibility of Singe Drops:
	2	28.06 +/- 0.19	26.73	3.5 +/- 0.1		
	3	27.13 +/- 0.10	25.77	7.0 +/- 0.2	d(IT)/dt	Volume: +/- 0.16uL
	4	26.56 +/- 0.20	25.18	10.3 +/- 0.5	(mN/ms):	Stroke: 1.9um
	5	26.12 +/- 0.27	24.73	12.6 +/- 0.9	-0.072	
	6	25.81+/- 0.03	24.42	15.4 +/- 0.3	Correlation:	
	7	25.61 +/- 0.29	24.21	17.7 +/- 1.2	0.9811	
	8	25.39 +/- 0.01	23.99	19.2 +/- 0.4		
	9	25.12 +/- 0.12	23.7	21.6 +/- 0.5		
	10	24.93 +/- 0.19	23.51	24.6 +/- 1.0		
	11	24.73 +/- 0.03	23.31	26.5 +/- 0.3		
	12	24.54 +/- 0.20	23.11	28.0 +/- 1.5		
	13	24.35 +/- 0.11	22.92	30.1 +/- 0.5		
		20.07 +/- 0.09				

Parameters and Notes were the same as those listed in Table 2Ba except for:

Svol:	5.0mL	syringe volume (containing HFE7100)
t:	0.07-0.40 (s/uL)	time allowed for drop to fall (this is the largest range)

APPENDIX C: TRACER EXPERIMENTS' DATA

Table C1: Tracer test results using acid yellow 17 in fracture 1. July 2004.

EFFLUENT DATA				
Time (min)	Absorbance at 400 nm	Conc (mg/L)	C/C_o (-)	C_f (-)
14.28	0.008	0.46	0.03	
29.37	0.003	0.28	0.02	0.00
45.80	0.003	0.28	0.02	0.08
55.52	0.013	0.63	0.04	0.33
74.98	0.051	1.97	0.12	0.62
85.62	0.099	3.67	0.22	0.64
101.45	0.177	6.42	0.25	0.75
112.37	0.272	9.77	0.38	1.31
117.12	0.304	10.90	0.42	1.21
129.15	0.387	13.82	0.54	1.12
144.55	0.444	15.83	0.62	1.07
155.20	0.49	17.45	0.68	1.23
165.30	0.544	19.36	0.75	1.39
176.53	0.608	21.61	0.84	1.35
187.62	0.642	22.81	0.89	1.20
198.50	0.668	23.73	0.92	1.19
210.68	0.695	24.68	0.96	1.19
231.75	0.735	26.09	1.02	1.24
248.93	0.768	27.26	1.06	1.22
284.53	0.808	28.67	1.12	1.26
321.50	0.857	30.39	1.18	1.30
368.37	0.896	31.77	1.24	1.55

INFLUENT DATA		
Time (min)	Absorbance at 400 nm	Conc (mg/L)
1.73	0.306	10.97
114.22	0.631	22.43
201.47	0.768	27.26
253.22	0.83	29.44
327.05	0.889	31.52
371.37	0.915	32.44
Average		25.68
Average (0-114min)		16.70

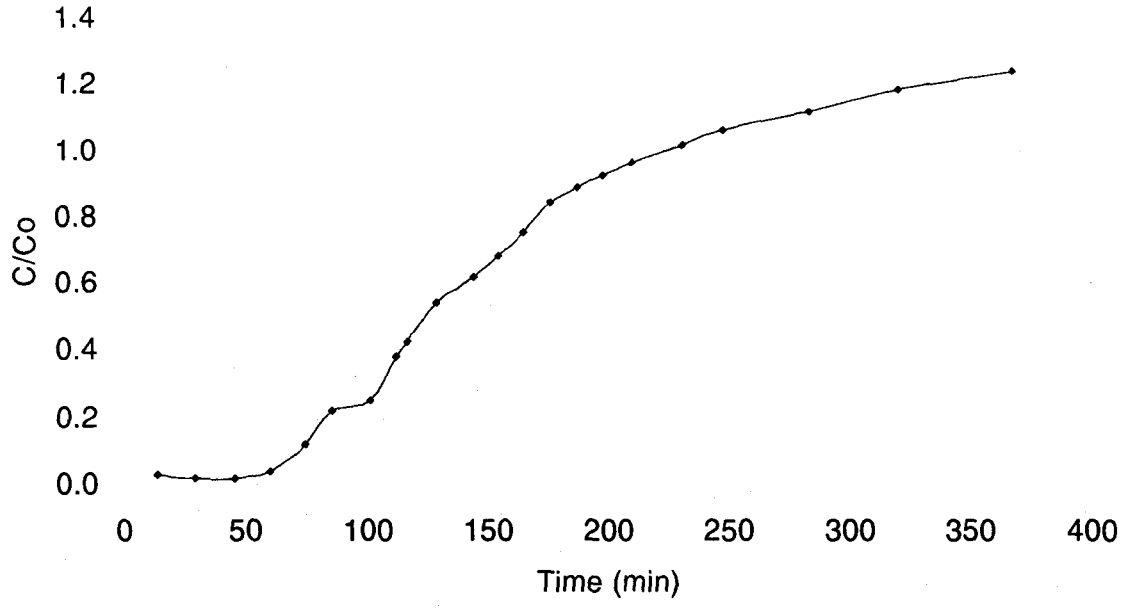

Figure C1: Raw data breakthrough curve for acid yellow 17 in fracture 1.

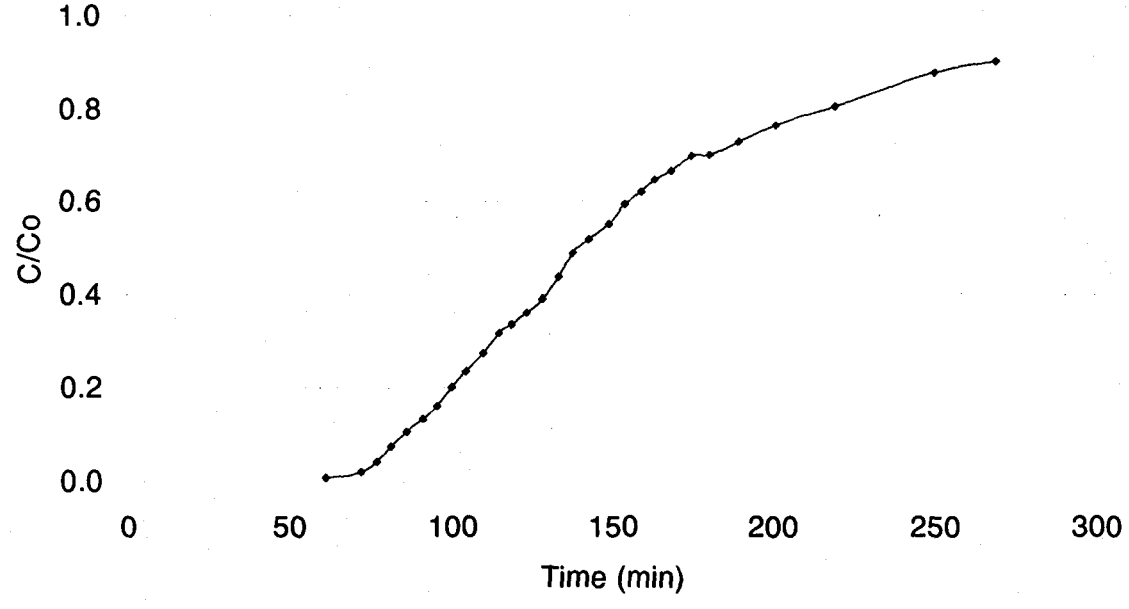

Figure C2: Raw data breakthrough curve for acid yellow 17 in fracture 2.

Table C2: Tracer test results using acid yellow 17 in fracture 2. August 2004.

EFFLUENT DATA				
Time (min)	Absorbance at 400 nm	Conc (mg/L)	C/C_o (-)	C_f (-)
61.27	0.002	0.25	0.01	
72.00	0.011	0.56	0.02	0.19
76.85	0.032	1.30	0.04	0.51
81.30	0.061	2.33	0.07	0.60
86.23	0.088	3.28	0.11	0.55
91.30	0.112	4.13	0.13	0.60
95.55	0.138	5.04	0.16	0.77
100.05	0.173	6.28	0.20	0.83
104.60	0.203	7.33	0.24	0.81
109.97	0.238	8.57	0.28	0.88
114.98	0.275	9.87	0.32	0.86
118.72	0.292	10.47	0.34	0.73
123.65	0.314	11.25	0.36	0.79
128.55	0.340	12.16	0.39	0.98
133.55	0.381	13.61	0.44	1.22
138.12	0.426	15.20	0.49	1.16
142.95	0.453	16.15	0.52	0.95
149.13	0.481	17.14	0.55	1.04
154.73	0.519	18.48	0.59	1.12
159.40	0.543	19.32	0.62	1.08
163.72	0.566	20.13	0.65	1.01
169.13	0.584	20.77	0.67	1.01
175.32	0.612	21.76	0.70	0.92
180.87	0.613	21.79	0.70	0.86
189.97	0.639	22.71	0.73	0.97
201.68	0.670	23.80	0.77	0.96
219.82	0.707	25.11	0.81	0.99
250.98	0.771	27.36	0.88	1.03
269.88	0.792	28.10	0.90	1.17

INFLUENT DATA		
Time from start (min)	Absorbance at 400 nm	Conc. (mg/L)
2.07	0.643	22.85
152.83	0.862	30.57
468.35	0.892	31.63
Average (last 2 samples)	0.877	31.10

APPENDIX D: INTERFACIAL TRACER EXPERIMENTS' DATA

Table D1: Effluent and influent concentrations in the interfacial tracer test, experiment 1 in fracture 1. June 2004.

EFFLUENT DATA									
SDBS					ACID YELLOW 17				
Time (min)	Area (counts)	Conc (mg/L)	C/Co (-)	Cf (-)	Time (min)	Abs. at 400nm (-)	Conc (mg/L)	C/Co (-)	Cf (-)
5.37	0	0.00	0.00		5.48	0	0.14	0.00	
8.73	0	0.00	0.00	0.00	10.32	0	0.14	0.00	0.01
12.27	0	0.00	0.00	0.00	15.55	0	0.18	0.00	0.08
17.17	0	0.00	0.00	0.00	20.63	0.009	0.49	0.01	0.10
21.85	0	0.00	0.00	0.00	27.02	0.012	0.60	0.02	0.11
25.78	0	0.00	0.00	0.00	32.67	0.024	1.02	0.03	0.32
28.75	0	0.00	0.00	0.00	38.35	0.054	2.08	0.05	0.47
32.20	0	0.00	0.00	0.00	43.98	0.083	3.10	0.08	0.54
36.02	0	0.00	0.00	0.00	48.73	0.114	4.20	0.11	0.57
40.37	451544	0.00	0.00	0.05	54.30	0.143	5.22	0.13	0.51
44.80	1747787	0.22	0.01	0.16	60.58	0.170	6.17	0.16	0.58
49.10	2499117	0.67	0.02	0.22	65.82	0.205	7.40	0.19	0.67
53.65	3248140	1.12	0.03	0.25	70.37	0.229	8.25	0.21	0.83
58.80	4279818	1.74	0.04	0.38	75.53	0.281	10.08	0.26	1.13
63.92	6100268	2.83	0.07	0.55	79.85	0.333	11.92	0.30	1.07
68.23	8055570	4.00	0.09	0.76	85.35	0.376	13.43	0.34	1.18
73.20	11168237	5.87	0.14	0.87	89.45	0.434	15.48	0.39	1.14
78.03	13972225	7.55	0.18	0.85	96.18	0.478	17.03	0.43	1.04
83.57	16875530	9.30	0.22	0.84	101.22	0.524	18.65	0.47	1.03
88.37	19272430	10.73	0.25	0.91	105.45	0.543	19.32	0.49	0.80
94.07	22576015	12.72	0.30	0.92	110.08	0.558	19.85	0.50	0.98
100.00	25213987	14.30	0.33	0.86	114.67	0.598	21.26	0.54	0.98
106.02	27752518	15.82	0.37	1.11	118.63	0.605	21.51	0.55	0.83
111.73	32306846	18.55	0.43	1.15	122.92	0.627	22.28	0.57	1.11
116.67	34021852	19.58	0.46	0.93	127.47	0.665	23.62	0.60	1.17
123.62	36911306	21.32	0.50	0.98	132.75	0.698	24.79	0.63	1.13
128.27	38560925	22.31	0.52	1.07	140.60	0.747	26.52	0.67	1.12
133.40	41285603	23.94	0.56	1.19	148.72	0.788	27.96	0.71	1.09
138.48	43855856	25.48	0.60	1.07	159.37	0.837	29.69	0.76	1.09
143.63	45306690	26.35	0.62	0.93	169.97	0.878	31.14	0.79	1.30
149.77	46766767	27.23	0.64	0.90	171.20	0.912	32.33	0.82	1.24
154.88	47759480	27.83	0.65	0.93	181.43	0.939	33.29	0.85	1.16
161.22	49370675	28.79	0.67	0.97	190.27	0.987	34.98	0.89	1.13
166.38	50582633	29.52	0.69	1.01	200.47	0.997	35.33	0.90	1.04
172.57	52326705	30.57	0.72	1.00	210.47	1.024	36.28	0.92	1.08
182.72	54354575	31.78	0.74	1.01	231.10	1.059	37.52	0.95	1.05
196.62	57585801	33.72	0.79	1.03	263.77	1.089	38.58	0.98	1.07

Table D1 continued: Effluent and influent concentrations in the interfacial tracer test, experiment 1 in fracture 1. June 2004.

EFFLUENT DATA									
SDBS					ACID YELLOW 17				
Time (min)	Area (counts)	Conc (mg/L)	C/Co (-)	Cf (-)	Time (min)	Abs. at 400nm (-)	Conc (mg/L)	C/Co (-)	Cf (-)
206.73	59093015	34.63	0.81	0.99	288.60	1.127	39.92	1.02	1.07
218.45	60712067	35.60	0.83	1.02	339.83	1.139	40.34	1.03	1.07
229.07	62493223	36.67	0.86	1.04	365.90	1.172	41.50	1.06	1.09
239.62	63820327	37.46	0.88	1.01	461.52	1.185	41.96	1.07	1.32
249.68	64806676	38.05	0.89	0.96					
260.55	65000169	38.17	0.89	0.94					
270.55	65667666	38.57	0.90	0.92					
292.75	65549353	38.50	0.90	0.95					
310.70	67352219	39.58	0.93	1.01					
331.53	68143658	40.06	0.94	1.00					
352.58	69397076	40.81	0.96	0.98					
372.73	69134580	40.65	0.95	0.98					
440.03	71192106	41.89	0.98	1.01					
513.00	72098769	42.43	0.99	1.00					
569.92	71349791	41.98	0.98	0.98					
657.12	72024032	42.38	0.99	1.00					
703.65	72189943	42.48	0.99	1.13					

INFLUENT DATA					
SDBS			ACID YELLOW 17		
Time (min)	Area (counts)	Conc (mg/L)	Time (min)	Abs. at 400nm (-)	Conc (mg/L)
1.52	65340706	38.37	1.67	0.733	24.47
41.70	64791102	38.04	55.70	0.891	29.61
89.65	66830281	39.27	106.57	0.965	32.01
144.97	69358461	40.78	171.20	0.985	32.66
231.67	72566717	42.71	212.20	1.020	33.80
441.42	72548960	42.70	232.90	1.190	39.32*
average (last 3): 42.06			*last sample used as Co		

Table D2: Effluent and influent concentrations the interfacial tracer, experiment 2 in fracture 1. July 2004.

EFFLUENT DATA									
SDBS DATA					ACID YELLOW 17 DATA				
Time (min)	Area (counts)	Conc (mg/L)	C/Co (-)	Cf (-)	Time (min)	Abs. at 400nm	Conc (mg/L)	C/Co (-)	Cf (-)
23.17	0	0.00	0.00		19.82	0.002	0.25	0.01	
31.63	0	0.00	0.00	0.00	26.27	0.002	0.72	0.02	0.13
37.85	0	0.00	0.00	0.00	32.62	0.002	0.72	0.02	0.02
43.25	0	0.00	0.00	0.00	39.27	0.002	0.72	0.02	0.05
49.18	1051907	0.00	0.00	0.18	47.48	0.006	0.85	0.03	0.63
55.12	2973874	0.95	0.02	0.54	49.18	0.066	2.80	0.09	2.53
61.40	6197490	2.89	0.07	0.73	52.45	0.136	5.07	0.16	1.33
67.77	9319217	4.76	0.12	0.75	56.82	0.162	5.92	0.18	0.63
73.32	11912504	6.32	0.16	0.66	60.00	0.172	6.24	0.19	0.72
79.17	13668419	7.37	0.19	0.72	65.70	0.212	7.54	0.23	1.00
85.65	16866162	9.29	0.24	0.93	71.55	0.267	9.33	0.29	1.26
90.90	19797802	11.05	0.29	0.92	76.17	0.321	11.08	0.34	1.17
96.27	22022282	12.38	0.32	0.86	85.18	0.388	13.26	0.41	1.27
102.12	24397873	13.81	0.36	1.01	91.57	0.462	15.67	0.49	1.28
110.78	29237937	16.71	0.43	1.14	97.38	0.492	16.64	0.52	0.89
116.10	31967373	18.35	0.47	1.17	103.20	0.509	17.19	0.53	0.66
122.47	35446317	20.44	0.53	1.18	108.18	0.507	17.13	0.53	0.71
127.67	37721816	21.80	0.56	1.24	114.90	0.532	17.94	0.56	0.94
132.73	40730070	23.61	0.61	1.24	122.32	0.565	19.01	0.59	1.01
140.37	43840122	25.47	0.66	1.25	128.82	0.594	19.96	0.62	0.98
145.82	46655319	27.16	0.70	1.27	135.15	0.615	20.64	0.64	1.04
152.88	49205691	28.69	0.74	1.19	143.02	0.655	21.94	0.68	1.03
158.58	50986328	29.76	0.77	1.16	154.77	0.688	23.01	0.71	0.96
173.57	55275986	32.33	0.84	1.13	166.20	0.716	23.92	0.74	0.98
185.38	56885557	33.30	0.86	1.07	177.63	0.747	24.93	0.77	0.97
195.65	58736193	34.41	0.89	1.15	188.27	0.763	25.45	0.79	0.98
205.98	60997644	35.77	0.93	1.14	199.27	0.792	26.39	0.82	1.01
216.17	62138539	36.45	0.94	1.04	219.18	0.828	27.56	0.85	0.99
227.00	62473346	36.65	0.95	1.08	257.98	0.876	29.12	0.90	0.99
252.23	65693793	38.58	1.00	1.12	310.33	0.918	30.48	0.94	1.00
289.88	68170511	40.07	1.04	1.12	367.20	0.939	31.17	0.97	1.00
311.33	69544738	40.90	1.06	1.12	442.92	0.963	31.95	0.99	1.01
353.73	71257382	42.01	1.09	1.11	484.57	0.967	32.08	0.99	1.00
436.73	73349105	41.92	1.09	1.10	561.10	0.974	32.30	1.00	1.19
518.87	74559589	43.18	1.12	1.33					

Table D2 Continued: Effluent and influent concentrations the interfacial tracer, experiment 2 in fracture 1. July 2004.

INFLUENT DATA					
SDBS DATA			ACID YELLOW 17 DATA		
Time (min)	Area (counts)	Conc (mg/L)	Time (min)	Abs. at 400nm (-)	Conc (mg/L)
0.87	39493574	22.86	1.40	0.76	25.19
88.03	55039032	32.19	94.10	0.89	29.44
147.98	63643938	37.36	174.87	0.96	31.88
314.37	71399390	42.01	456.43	0.98	32.47
523.15	73026503	42.98	566.90	0.98	32.43
average: 38.64			average of last three samples: 32.26		

Table D3: Effluent and influent concentrations for the interfacial tracer test, experiment 2 in fracture 2. August 2004.

EFFLUENT DATA									
SDBS					ACID YELLOW 17				
Time (min)	Area (counts)	Conc (mg/L)	C/Co (-)	Cf (-)	Time (min)	Abs. at 400nm (-)	Conc (mg/L)	C/Co (-)	Cf (-)
59.65	344805	0.00	0.00		48.15	0.013	1.07	0.03	
63.95	80028	0.00	0.00	0.00	54.75	0.004	0.78	0.02	0.00
67.77	975354	0.00	0.00	0.00	60.40	0.007	0.88	0.03	0.13
73.20	827936	0.00	0.00	0.10	67.08	0.021	1.33	0.04	0.24
77.57	1935184	0.33	0.01	0.36	72.57	0.040	1.95	0.06	0.21
81.92	3150071	1.06	0.04	0.51	79.52	0.046	2.15	0.07	0.26
86.28	4369151	1.79	0.07	0.64	86.90	0.078	3.19	0.10	0.71
90.52	6080278	2.82	0.10	0.71	91.40	0.146	5.40	0.16	1.15
95.35	7628019	3.75	0.14	0.71	96.30	0.206	7.35	0.22	0.38
100.20	9331059	4.77	0.18	0.91	101.53	0.168	6.11	0.19	-0.18
105.95	12255415	6.52	0.24	0.98	108.03	0.147	5.43	0.16	0.09
111.30	14211760	7.70	0.28	0.72	115.92	0.154	5.66	0.17	0.46
117.60	15268745	8.33	0.31	0.67	121.32	0.200	7.15	0.22	0.67
123.07	16718710	9.20	0.34	0.66	130.13	0.243	8.55	0.26	0.67
132.27	18096079	10.03	0.37	0.72	140.10	0.305	10.56	0.32	0.75
140.05	20269316	11.33	0.42	0.98	149.88	0.361	12.38	0.38	0.77
149.72	23896797	13.51	0.50	1.01	162.43	0.425	14.46	0.44	0.81
161.58	26835586	15.27	0.56	0.84	173.10	0.480	16.25	0.49	0.82
171.57	27562405	15.71	0.58	0.62	184.40	0.525	17.71	0.54	0.87
182.57	27351420	15.58	0.57	0.68	200.05	0.603	20.25	0.61	0.94
199.65	29356879	16.78	0.62	0.87	217.68	0.676	22.62	0.69	0.94
214.13	32063921	18.41	0.68	0.90	232.10	0.713	23.82	0.72	0.92
244.70	35387242	20.40	0.75	0.94	252.28	0.772	25.74	0.78	0.97
282.92	40002666	23.17	0.85	0.94	274.80	0.825	27.46	0.83	1.00
349.37	40986238	23.76	0.87	0.90	294.97	0.871	28.96	0.88	0.99
415.98	41999380	24.37	0.89	0.97	326.03	0.907	30.13	0.91	1.00
478.55	46793342	27.25	1.00	1.17	373.57	0.965	32.01	0.97	1.04

Table D3 Continued: Effluent and influent concentrations for the interfacial tracer test, experiment 2 in fracture 2. August 2004.

INFLUENT DATA					
SDBS			ACID YELLOW 17		
Time (min)	Area (counts)	Conc (mg/L)	Time (min)	Abs. at 400nm (-)	Conc (mg/L)
3.43	66508122	39.07	157.65	1.053	34.87
125.18	66670401	39.17	341.93	1.104	36.53
219.50	75690916	44.58	533.67	1.112	36.79
487.13	75900553	44.71			
average(first 2 samples): 39.12 total average: 41.88			average(last 3 samples): 32.96		

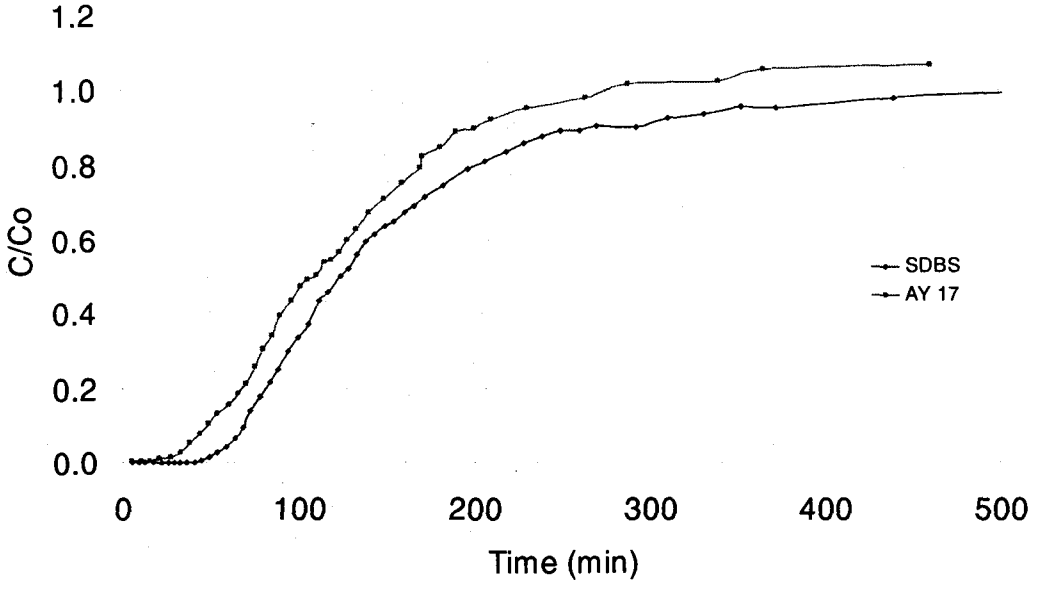

Figure D1: Breakthrough curves for raw data of experiment 1 in fracture 1.

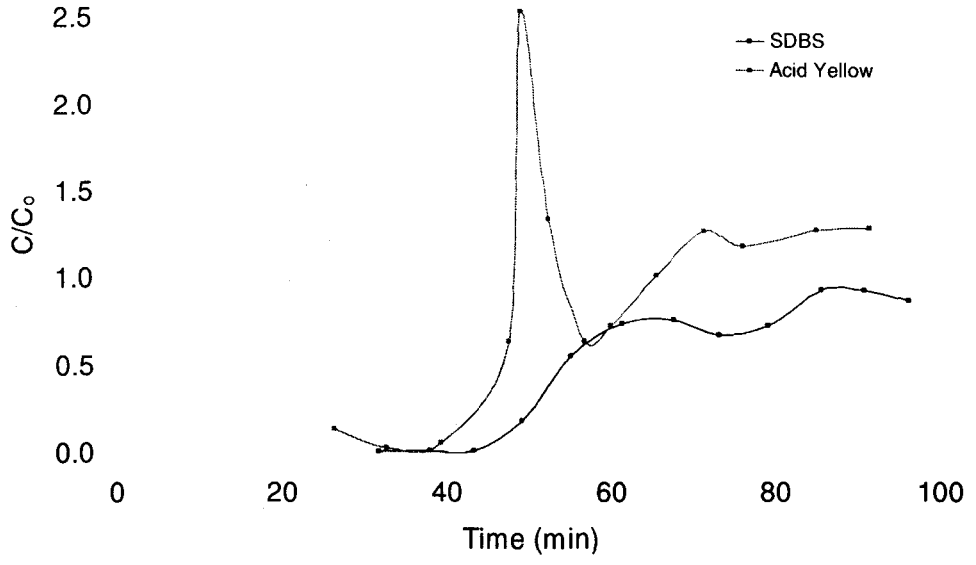

Figure D2: Breakthrough curves for raw data of experiment 2 in fracture 1.

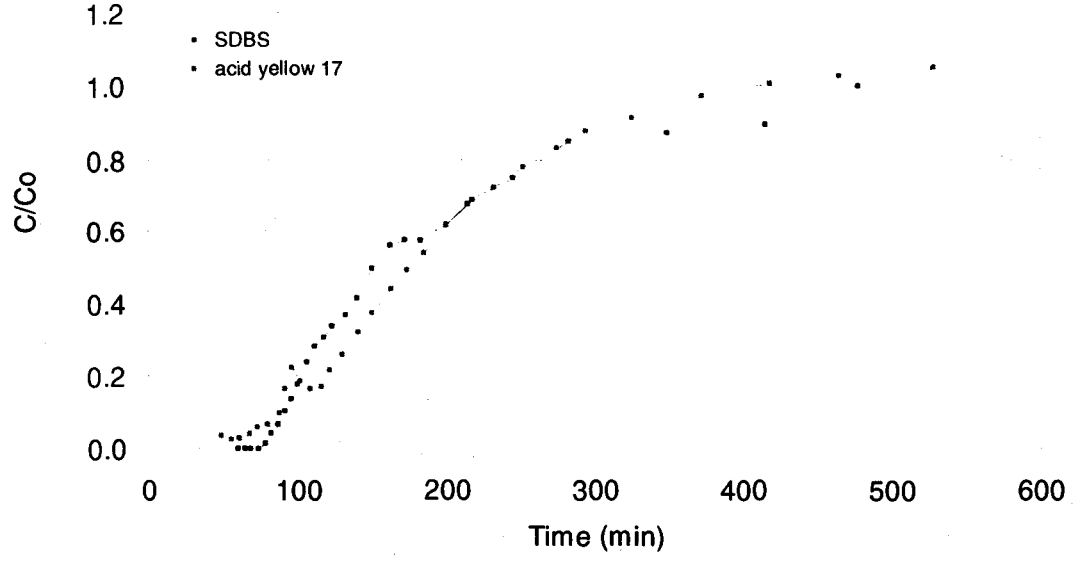

Figure D3: Breakthrough curves for raw data of experiment 3 in fracture 2.